ISTANBUL TECHNICAL UNIVERSITY ★ GRADUATE SCHOOL OF SCIENCE ENGINEERING AND TECHNOLOGY

INVESTIGATION ON THE EFFECT OF HEAT AFFECTED ZONES OVERLLAPING IN MULTIPASS TIG WELDING OF AUSTENETIC STAINLESS STEEL PIPES

M.Sc. THESIS

Arash ARMANFAR

Department of Mechanical Engineering

Mechanical design M.Sc. Programme

June 2018

ISTANBUL TECHNICAL UNIVERSITY ★ GRADUATE SCHOOL OF SCIENCE ENGINEERING AND TECHNOLOGY

INVESTIGATION ON THE EFFECT OF HEAT AFFECTED ZONES OVERLLAPING IN MULTIPASS TIG WELDING OF AUSTENETIC STAINLESS STEEL PIPES

M.Sc. THESIS

Arash ARMANFAR
(503141227)

Department of Mechanical Engineering

Mechanical design Programme

Thesis Advisor: Prof. Dr. Mehmet PALABIYIK

MAY 2018

İSTANBUL TEKNİK ÜNİVERSİTESİ ★ FEN BİLİMLERİ ENTİTÜSÜ

ÖSTENİTİK PASLANMAZ ÇELİK BORULARIN MULTIPASS TIG KAYNAKLARİNDA İSİDAN ETKİLENEN BÖLGELERIN ÜST ÜSTE GELMESININ ETKİSİNİN İNCELENMESİ

YÜKSEK LİSANS TEZİ

Arash ARMANFAR
(503141227)

Makine muhendisligi Anabilim Dalı

konstroksiyon Yüksek Lisans Programı

Tez Danışmanı: Prof. Dr. Mehmet PALABIYIK

MAYIS 2018

Arash ARMANFAR, a M.Sc. student of ITU Graduate School of Arts and Social Sciences student ID 503141227, successfully defended the thesis/dissertation entitled "**INVESTIGATION ON THE EFFECT OF HEAT AFFECTED ZONES OVERLLAPING IN MULTIPASS TIG WELDING OF AUSTENETIC STAINLESS STEEL PIPES**", which he prepared after fulfilling the requirements specified in the associated legislations, before the jury whose signatures are below.

Thesis Advisor :	**Dr. Mehmet PALABIYIK** Istanbul Technical University	.....
Jury Members :	**Prof. Dr. Cemal Baykara** Istanbul Technical University	.....
	Prof. Dr. Cuneyt FETVACI Istanbul University	.....

Date of Submission : 26 April 2018
Date of Defense : 4 June 2018

To my family,

FOREWORD

This thesis is dedicated to my family, specially my mother, who has always been beside me throughout all seconds of my life. I appreciate all of their love, patience and never-ending support through my life.

I would like to express my sincere appreciation to my percious advisor Dr. Mehmet PALABIYIK for his patience, technical guidance, support and his warm encouragmenet that pushes me beyond my boundries.

I would also like to thank my dear friend TUNÇ IŞIKLI for his help and support through experimental works although having a busy scheduale. I wish to thank people from TÜPRAŞ (Turkey's only oil refiner), specially ÖZGÜR KÖSE, for their support and guidance during experimental tests.

I would aslo like to express my deepest appreciation to my dear brother, AIDIN ARMANFAR who has supported and helped me not only through all the phases of preparing this thesis but also in all steps of my life.

To all of you thank you very much.

May 2018

Arash ARMANFAR
(Mechanical Engineer)

TABLE OF CONTENTS

Page

FOREWORD ..... **ix**
TABLE OF CONTENTS ..... **xi**
ABBREVIATIONS ..... **xiii**
SYMBOLS ..... **xv**
LIST OF TABLES ..... **xvii**
LIST OF FIGURES ..... **xix**
SUMMARY ..... **xxiii**
ÖZET ..... **xxv**
1. INTRODUCTION **1**
1.1 Definition of Problem 1
1.2 Purpose of Thesis 2
2. FUNDAMENTALS **3**
2.1 Tungsten Inert Gas Welding (TIG) 3
2.1.1 Polarity in GTAW 4
2.1.2 Shielding gasses in GTAW 5
2.1.3 Multi-pass TIG Welding 6
2.1.4 Advantages and disadvantages of GTAW 6
2.2 Heat Affected Zone (HAZ) 7
2.2.1 HAZ sub-zones in single pass welding 9
2.2.2 HAZ subzones in multi-pass welding 10
2.3 Parameters Controlling Heat Affected Zone Width and Properties 11
2.3.1 Material welded 11
2.3.2 Thickness and cooling rate 11
2.3.3 Heat input and maximum temperature 12
2.4 Austenitic stainless-steel pipes 13
3. WELDING FINITE ELEMNENT ANALYZING **15**
3.1 Introduction 15
3.2 Physical Modeling and mesh generation 18
3.3 Material Properties 19
3.4 Thermal Analysis 20
3.4.1 Governing equation 20
3.4.2 Heat input condition 21
3.4.3 Boundary conditions 24
3.5 Mechanical Analysis 24
3.6 FEM Results 26
3.6.1 Temperature cycles 26
3.6.1.1 Pipe number 1: Temperature cycles in inner and outer surfaces 27
3.6.1.2 Pipe number 2: Temperature cycles on inner and outer surfaces 29
3.6.1.3 Pipe number 3: Temperature Cycles for outer and inner surfaces 31
3.6.1.4 Pipe number 4: Temperature Cycles at outer and inner surfaces 33
3.6.2 Residual Stress Distribution 35
3.6.2.1 Pipe Number 1: axial and hoop residual stress distribution 36

3.6.2.2 Pipe Number 2: axial and hoop stress distribution 37
3.6.2.3 Pipe Number 3: Axial and Hoop stress distribution 38
3.6.2.4 Pipe Number 4: Axial and Hoop Stress distribution 39
3.6.3 HAZ ranges 40
4. EXPERIMENTAL WORKS 42
4.1 Material and methods 42
4.1.1 Welding Proccess and Material 42
4.1.2 Hardness Test 43
4.1.3 Tensile Testing 44
4.1.4 Charpy Impact Testing 46
4.2 RESULTS AND DISCUSSION 47
4.2.1 Hardenss test results 47
4.2.2 Tensile test results 48
4.2.3 Charpy Impact Test resuts 49
5. CONCLUSIONS 52
REFERENCES 54
APPENDICES 58
APPANDIX A.1: 59
APPANDIX A.2: 61
APPANDIX A.3: 64
APPANDIX A.4: 68
APPANDIX A.5: 73
CURRICULUM VITAE 74

ABBREVIATIONS

HAZ	**:** Heat Affected Zone
FZ	**:** Fusion Zone
FEA	**:** Finite Element Analysis
TIG	**:** Tungesten Inert Gas
GTAW	**:** Gass Tungesten Arc Welding
CGHAZ	**:** Coarse Grain Heat Affected Zone
FGHAZ	**:** Fine Grain Heat Affected Zone
ICHAZ	**:** Inter Critical Heat Affected Zone
SCHAZ	**:** Sub Critical Heat Affected Zone
ICHAZ	**:** Inter Critical Heat Affected Zone
SCHAZ	**:** Sub Critical Heat Affected Zone

SYMBOLS

$\boldsymbol{\alpha}$	**:** Thermal diffusivity
$\boldsymbol{T_x}$	**:** Recrystallization Temperature
$\boldsymbol{\rho}$	**:** Density
$\boldsymbol{k_x, k_y, k_z}$	**:** Thermal Conducticty Components
$\boldsymbol{c_p}$	**:** Specific heat capacity
t	**:** Time
Q	**:** Heat Input
V	**:** Voltage
I	**:** Current
s	**:** Speed
$\boldsymbol{\mu}$	**:** Arc efficiency
ρ	**:** Density
$\sigma_x, \sigma_y, \sigma_{xy}$	**:** Shell internal stresses

LIST OF TABLES

Page

Table 2.1: Properties of inert gasses [2]. **5**
Table 2.2: HAZ sub-zones in single pass welding. [5] **9**
Table 2.3: two pass welding HAZ subzones definition **10**
Table 2.4: Chemical composition of Austenitic stainless stell304L. [13] **14**
Table 3.1: Geometrical information of pipes **19**
Table 3.2: Mechanical and Thermal Properties of Austenitic Stainless Steel 304L. **20**
Table 3.3: Welding Condition **22**
Table 3.4: HAZ lengths for Pipes welding **40**
Table 4.1: Tensile Test Results **49**
Table 4.2: Impact toughness measures. **50**

LIST OF FIGURES

Page

Figure 1.1: two close welds. **1**
Figure 2.1: TIG Welding equipments and process [1] **4**
Figure 2.2: different types of polarity in TIG welding [1]. **5**
Figure 2.3: the temperature distribution during the TIG welding of a S30432 stainless steel pipe. [4] **7**
Figure 2.4: effect of Temperature cycles on hardness and strength of base metal. [1] **8**
Figure 2.5: Schematic of the sub-zones of the HAZ corresponding to the calculated equilibrium phase diagram of P91-type steel. [5] **9**
Figure 2.6: Schematic of the sub-zones of the HAZ in two pass welding **10**
Figure 2.7: effect of input on HAZ properties. [1] **12**
Figure 2.8: schematic diagram of the various sub-zones of the heat-affected zone approximately corresponding to the alloy (0.03 wt% Carbon) indicated on the Fe-Fe3C equilibrium diagram **14**
Figure 3.1: Physical phenomena involved and their couplings [20]. **17**
Figure 3**.2:** meshed model. **18**
Figure 3.3: Mirrored Model. **19**
Figure 3.4: Goldak propsed heat distribution. [24] **22**
Figure 3.5: Pipes welding information: (a)PIPE Number 1, (b) PIPE Number 2, (c) Pipe number 3 and (d) Pipe number 4. **23**
Figure 3.6: Thermal cycles at three locations on the inside surface at 2mm from the weld center for Pipe 1 **27**
Figure 3.7: Thermal cycles at three locations on the inside surface at 4mm from the weld center for Pipe 1 **27**
Figure 3.8: Thermal cycles at three locations on the inside surface at 10mm from the weld center for Pipe 1 **27**
Figure 3.9: Thermal cycles at three locations on the inside surface at 20mm from the weld center for Pipe 1 **27**
Figure 3.10: Thermal cycles at three locations on the outside surface at 3mm from the weld center for pipe 1. **28**
Figure 3.11: Thermal cycles at three locations on the outside surface at 5mm from the weld center for pipe 1. **28**
Figure 3.12: Thermal cycles at three locations on the outside surface at 10mm from the weld center for pipe 1. **28**
Figure 3.13: Thermal cycles at three locations on the outside surface at 15mm from the weld center for pipe 1. **28**
Figure 3.14: Thermal cycles at three locations on the inside surface at 2.5mm from the weld center for pipe 2. **29**
Figure 3.15: Thermal cycles at three locations on the inside surface at 5.5mm from the weld center for pipe 2 **29**
Figure 3.16: Thermal cycles at three locations on the inside surface at 10mm from the weld center for pipe 2. **29**

Figure 3.17: Thermal cycles at three locations on the inside surface at 14mm from the weld center for pipe 2. **29**
Figure 3.18: Thermal cycles at three locations on the outside surface at 3.5mm from the weld center for pipe 2. **30**
Figure 3.19: Thermal cycles at three locations on the outside surface at 6mm from the weld center for pipe 2. **30**
Figure 3.20: Thermal cycles at three locations on the outside surface at 10mm from the weld center for pipe 2. **30**
Figure 3.21: Thermal cycles at three locations on the outside surface at 14mm from the weld center for pipe 2. **30**
Figure 3.22: Thermal cycles at three locations on the inside surface at 4.5mm from the weld center for pipe 3. **31**
Figure 3.23: Thermal cycles at three locations on the inside surface at 10mm from the weld center for pipe 3. **31**
Figure 3.24: Thermal cycles at three locations on the inside surface at 15.5mm from the weld center for pipe 3. **31**
Figure 3.25: Thermal cycles at three locations on the inside surface at 19.5mm from the weld center for pipe 3. **31**
Figure 3.26: Thermal cycles at three locations on the outside surface at 5mm from the weld center for pipe 3. **32**
Figure 3.27: Thermal cycles at three locations on the outside surface at 10mm from the weld center for pipe 3. **32**
Figure 3.28: Thermal cycles at three locations on the outside surface at 15.5mm from the weld center for pipe 3. **32**
Figure 3.29: Thermal cycles at three locations on the outside surface at 19.5mm from the weld center for pipe 3. **32**
Figure 3.30: Thermal cycles at three locations on the inside surface at 5mm from the weld center for pipe 4. **33**
Figure 3.31: Thermal cycles at three locations on the inside surface at 10mm from the weld center for pipe 4. **33**
Figure 3.32: Thermal cycles at three locations on the inside surface at 20mm from the weld center for pipe 4. **33**
Figure 3.33: Thermal cycles at three locations on the outside surface at 25mm from the weld center for pipe 4. **33**
Figure 3.34: Thermal cycles at three locations on the outside surface at 7mm from the weld center for pipe 4. **34**
Figure 3.35: Thermal cycles at three locations on the outside surface at 13.5mm from the weld center for pipe 4. **34**
Figure 3.36: Thermal cycles at three locations on the outside surface at 20mm from the weld center for pipe 4. **34**
Figure 3.37: Thermal cycles at three locations on the outside surface at 25mm from the weld center for pipe 4. **34**
Figure 3.38: Axial stress distribution for various orientations from weld center on the inside surface for pipe 1. **36**
Figure 3.39: Axial stress distribution for various orientations from weld center on the outside surface for pipe 1. **36**
Figure 3.40: Hoop stress distribution for various orientations from weld center on the inside surface for pipe 1. **36**
Figure 3.41: hoop stress distribution for various orientations from weld center on the outside surface for pipe 1. **36**

Figure 3.42: Axial stress distribution for various orientations from weld center on the inside surface for pipe 2.....**37**
Figure 3.43: Axial stress distribution for various orientations from weld center on the outside surface for pipe 2.....**37**
Figure 3.44: Hoop stress distribution for various orientations from weld center on the inside surface for pipe 2.....**37**
Figure 3.45: hoop stress distribution for various orientations from weld center on the outside surface for pipe 2. .....**37**
Figure 3.46: Axial stress distribution for various orientations from weld center on the inside surface for pipe 3.....**38**
Figure 3.47: Axial stress distribution for various orientations from weld center on the outside surface for pipe 3.....**38**
Figure 3.48: Hoop stress distribution for various orientations from weld center on the inside surface for pipe 3.....**38**
Figure 3.49: hoop stress distribution for various orientations from weld center on the outside surface for pipe 3. .....**38**
Figure 3.50: Axial stress distribution for various orientations from weld center on the inside surface for pipe 4.....**39**
Figure 3.51: Axial stress distribution for various orientations from weld center on the outside surface for pipe 4.....**39**
Figure 3.52: Hoop stress distribution for various orientations from weld center on the inside surface for pipe 4.....**39**
Figure 3.53: hoop stress distribution for various orientations from weld center on the outside surface for pipe 4. .....**39**
Figure 4.1 prepared welding models.....**42**
Figure 4.2: Welded Pipes. **43**
Figure 4.3: PROCEQ Equotip Bambino 2 Portable Hardness tester collibration. **44**
Figure 4.4: Tensile test samples. **45**
Figure 4.5: ASLA Universal Tensile Test Machine. **45**
Figure 4.6: Different regions in teh final step **46**
Figure 4.7: Impact Test samples geometry **46**
Figure 4.8: Prepared Charpy Impact Test samples.....**47**
Figure 4.9: ASLA 450J Impact Test Machine. **47**
Figure 4.10: Hardness measured zones.....**48**
Figure 4.11: Measured Hardness For different zone **48**
Figure 4.12: Fracture Locations **49**

INVESTIGATION ON THE EFFECT OF HEAT AFFECTED ZONES OVERLLAPING IN MULTIPASS TIG WELDING OF AUSTENETIC STAINLESS STEEL PIPES

SUMMARY

Multipass Tungesten Inert Gas (TIG) welding is one of the popular weld processes employed to join austenitic stainless steel pipes in industrial sites like refineries and petrochemical industries. Since experiencing intensive temperature cycles and residual stresses as a result of high heating, Heat Affected Zone is a volnurable region which is threatened by various types of crackings and defects in welding. In the pipeline designs and fittings because of different reasons, in some cases, the distance between two consecutive multipass butt welds are too much small that generated HAZ's from welds, may be overlapped in the tiny pipe located in the middle of two other parts. Reports reveal that there are leakages from these HAZ's overlapping sections. The aim of this study was to investigate the influence of overlapping of HAZ's, generated from two consecutive close welds, on the mechanical behavior of TIG welded 304L austenitic stainless steel pipes with different outer diameters and wall thicknesses.

In this investigation, four pipes are selected to be studied. Two pipes with the same outer diameter of 2" but different schedule numbers of 40 and 80. And two the other pipes have the outer diameter of 4" and schedule numbers of 80 and 120. In the fist step, a 3D finite element model was created for multipass welding mentioned four pipes. Considering the thickness of pipes, number of applied weld passes were chosen (2,3,4 and 6 passes). all the analysis has been done in ABAQUS software. Base on FEA, the transient temperature distributions and both axial and hoop residual stress distribution on inside and outside of pipes in different orientations were plotted for all the pipes. The results show that the temperature and residual stresses distribution are constant in different orientations through the pipes (90°.180°.270° from the welding start point). For all the samples, on the outer surface, axial residual stress are comperasive in fusion zone and by getting away from the FZ it is changing to tensile situation. The reverese situation can be seen in the inside surface where the axial residual stress is tensile in the FZ and growing comperasive by distance from FZ. For the hoop stress at the weld zone and its vicinity larg tensile stresses are produced in outer and inner surfaces. By studing Temperature cycles, the length of Heat affected zones are identified for multipass TIG welding of pipes with different number of welding passes. In the next step, these obtained lengths were applied in experimental tests, for each size of pipes, a small pipe with a length equals to two times the length of related measured HAZ length was provided. Then, these small pipes were TIG welded to two other pipes with the same sizes but larger lengths from bothsides. The situation of welding (number of passes, current, voltage and speed of welding for each pass) was same as the finite elemenet analysis. In the next step, mechanical testes were carried out to investigate the behavior of the material under HAZ's overlapping. Hardness investigations declare that in these sections hardness reaches to the maximum value. All the samples, except the one related to the pipe 2" with schedule number 40, were factured from the overlapping section and a small decrease in brittle

toughness of material were detected in the overlappimng section. Tensile residual stresses and effect of reheating have the biggest effects on these abatements in mechanical properties. Overally it can be conculuded that HAZ's overlapping isnot a desirable situation and it shoud be better to avoid too close butt welds in the multipass TIG welding of austenitic stainless steel pipes.

ÖSTENİTİK PASLANMAZ ÇELİK BORULARIN MULTIPASS TIG KAYNAKLARİNDA İSİDAN ETKİLENEN BÖLGELERIN ÜST ÜSTE GELMESININ ETKİSİNİN İNCELENMESİ

ÖZET

Buhar santralleri, rafineri ve yer altı-yer üstü doğal gaz transferi için. Borular ve borulama parçaları çok sık kulanılmaktadır. Belli boylarda imalatı yapılan boruların birleştirilmesi için kaynaklı imalat yöntemi uygunlanmaktadır. İki adet borunun çevresel olarak birlestirilmesi için borularin et kalınlığı ve çapına bağlı olarak farklı kaynak yöntemleri uygulanmaktadır. Küçük çapa sahip (maximum 4 inç) boru kaynaklarında, en sık kullanılan kaynak yöntemise TIG (Tungesten Inert Gas) kaynağıdır. TIG kaynağında, yüksek sıcaklık döngüleri nedeniyle, Isı Tesiri Altında Kalan Bölgeler üretilir. Isı Tesiri Altında Kalan Bölge (ITAB), yüksek sıcaklığın parçayı eritmek için çok düşük olduğu ancak malzemelerin mikroyapısını ve özelliklerini önemli ölçüde değiştirecek kadar yüksek olduğu bir metal parçasıdır. ve bu bölge kaynağın en hassas kısımlarından biridir. ITAB'ın (ve bunun alt bölgelerinin) boyutu ve özellikleri, baz metalin özellikleri, parça kalınlığı, gerçekleştirilen kaynak işlemi, kaynak süresi, maksimum sıcaklık, kaynak arkının lineer elektrik enerjisinin değeri, kaynak koşulları, soğutma verimliliği gibi birçok faktöre bağlıdır. Kaynak dolgu metal türü, ısı girişi ve diğerleri. ITABin boyutunun ve özelliklerinin belirlenmesi ve kontrol edilmesi, sonuçtaki kaynakların daha kabul edilebilir olmasını sağlar.

İki farlkı çeversel boru kaynağının birbirine çok yakın olması sebebiyle, rafineri ve buhar santralleri gibi yüksek sıcaklık ve basıncın olduğu işlemelerde, mevcüt boru hatlarında devreye alınma sonrası kaçaklar yaşanmaktadır. Kaynaklar arası mesafenin az olması, ve ısının tesiri altında olan bölgelerin üst üste gelmesi bu kaçaklara sebep olduğu düşünülmektedir. Uluslararası, Standard, kod ve prosedürlerde iki kaynak arasında minimum mesafeyle ilgili bir madde veya görüş bulunmamaktadır. Kaynaklar arasında minimum mesafenin gerekli olduğu, hem yaşanan kaçaklardan hem de iki adet ITAB'n üst üste binilmesinen dolayı, ana malzemenin mekanik özelliklerini kötüleştirdiği düşünmektedir.

Bu porojede östenetik paslanmaz çeliği (304L) farkli et kalınlığı ve çaptaki boruların TIG kaynak için ITAB genişliklerinin belirnemesi, sonrasındada ITAB üst üste binmesi sonrası mekanik özelliklerde değişimleri incelenmesi amaçlandırılma istemektedir. Bu çalışmada farklı dış çapı ve et kalınlıklarına sahip dört adet 304L boru incelenmiştir. Bu boruların ikisinin dış çapı 2 inç schedule numarası 40 ve 80 dır diğer iki borunan dış çapı 4 inç ve schedule numaraları 80 ve 120 dır. Kullandığımız kaynak yöntemi TIG kaynağıdır. Boruların et kalınlıklarını düşünerek, paso sayısı belirlenmiştir. Et kalınlığı arttıkca paso sayısı çoğalmakta olup en kalın boru için kaynak 6 pasoda yapılacaktı.

İlk adımda, her bir boru için, ABAQUS yazılımında, bir üç boyutlu sonsuz elemanlar modeli hazırlayarak ve Kaynağın similasiyonunu yaparak, boruların kaynak yapılan zaman ısı dağılımı çizelgeleri ve bu yüksek ısı girişinen ve soğumadan ortaya çıkan

eksenel ve çevresel artık gerilmelerin dağlımı elde edilmiştir. Pratik olarak kaynak işlemi, bir çift termo-mekanik olaydır ancak mekanik kısımı, ihmal edilebilir ters bağımlılık ile termal alanına büyük ölçüde bağımlıdır bu sebeble birleştirilmemiş analiz çok dakik sounuçlara yol açıyor. Analiz prosedürü iki aşamaya ayrılabilir. İlk olarak, kaynak modelindeki sıcaklık dağılımı ve geçmişi ısı iletim analizi ile hesaplanır. Daha sonra sıcaklık geçmişi, artık gerilme alanının sonraki mekanik elastik plastik hesaplamasında bir termal yük olarak kullanılır. Kaynak işleminde ısı transferi bir geçici ısı transfer kılıfıdır, bu yuzden zamana bağlı ısı transferi denklemi, kaynağın termal analizinde yönetim denklemidir.

Kaynak torçunun hareketinin ve ısı dağılımını modelemek için Goldak tarafından önerilen "çift elipsoid" model FORTRAN'de kod olarak yazılmıştır. Boruda yaşanan ısı kayıbınn sebebi olarak radiyasiyon ve konveksiyon kayıplarının ikisida bu tezde içerilmektedir. Radiyasiyon kayıplar, kaynak bölgesine yakın olan yüksek sıcaklıklarda (500°C'den daha fazla olan bölgeler) öne çıkmakda olarak, konveksiyon kayıpları kaynağa daha uzak, nisbeten düşük sıcaklıklarda öne çıkmaktadır. bu sınır şartlarını uygulamak için, sıcaklığa bağlı bir katsayı, FORTRAN'de yazılan kodlar yardımıyla boruların, kaynak bölgesi dahil, tüm yüzeylerine uygulanmıştır. Bu çalışmada "elements birth and death" adlı yöntem kaynak sırasında kullanılmıştır. Böyle ki, ilk paso yapılan zaman ikinci paso etkisiz olup (havanin özelliklerine sahiplendirinip), birinci paso bitikden sonra ikinci paso devreye giriyor. Bu prosedür tüm pasolar arasında uygulanmıştır. Pasolar arasında sıcaklığın 25° düşünceye kadar, bir bekleme süreci vardır. Mekanik analiz, termal analizde kullanılan aynı örgü modeli ile gerçekleştirilir. Bu adımda analiz, termal analiz ile hesaplanan sıcaklık geçmişlerini giriş verileriyle gerçekleştirmektedir. Katı haldeki faz dönüşümü, kaynak sırasında paslanmaz taban metalinde ve kaynak metali içinde meydana gelmediğinden, toplam gerilme oranı üç bileşene ayrılabilir. Elastik gerginlik, izotropik Hooke'un kanoonunun sıcaklığa bağlı Young's modülü ve Poisson oranı ile modellenir ve termal Strain, ısıya bağlı ısıl genleşme katsayısı kullanılarak hesaplanır. Plastik gerginlik için, orandan bağımsız plastik model aşağıdaki özelliklere sahiptir: sıcaklığa bağlı mekanik özellikler ve doğrusal kinematik sertleştirme modeli. Bu araştırmada takip edilen FEA prekürsyonu önceki çalışmaların çoğunda doğrulanmıştır ve sonuçlar deneysel çalışmalarla iyi bir uyum içindedir.

Sonsuz elemanlar analizlerinden alınan sonuçları inceledikten sonra. ısı dağılımının boruların cevresel yüzeylerinde sabit olduğu görunuyor. Malzemenin düşük bir sıcaklık iletkenliğe sahip olmasi ve kaynak hızının yüksek olması bu konunun açıklaması olarak düşünümekdir. Kalınlık arttıkca, paso sayısı arttmakda olup bunun sonucunda borular daha fazla ısı etkisi altında kalarak, ITAB bölgesinin genişliği arttmaktadır. FEA den alınan sonuçlara göre, dış yüzeylerde eksenel artık gerilme füzyon bölgesinde basma formundadır, ancak kaynak merkezindan uzaklaşınca bu gerilme çok hızlı bir şeklide çekme haline gelmektedir. borunun iç tarafında bunun tam tersi görünmektedir, kaynak merkezinde çekme halinde olup, uzaklaşarak basma formuna girmektedir. çevresel artık gerilmeye bakıldığında, kaynak merkezi ve ITAB da, borunun dış ve iç yüzeylerin ikisindede, yüksek çekme halindedir. Isı dağılımlarını inceliyerek, ITAB bölgesinin uzunluğunu belli edıyoruz. Litraturden alındığı standarda göre, kullanılan malzeme için, 550°C den daha fazla (erime noktasına kadar) sıcaklıklar tesiri altında kalan bölgeler, ITAB bolgesi olarak belirlendi. Bir sonraki adimda belirlenen ITAB uzunluklarına göre deneysel çalışmalar yapıldı.

Dört borudan her birisi için, hesaplanan ITAB uzunluğunun iki katı uzunluğunda ve aynı dış çapı ve et kalınlığına sahip bir küçük boru üretilmiştir. Sonraki adımda belirlenen paso sayısında, iki tarafından iki boruya kaynatılmıştır. Besleme elktrodı

308L ve koruyucu gaz argon gazı 12-15 litre/dakika akış hızlıyla olmakta, modelemede kullanılan kaynak yöntemi, ayarları ve parametrelerinın aynısı uygulanmıştır. Son olarak mekanik özelliklerini belilerlemek için farklı testler yapıldı. Bu çalışmada farklı kaynak bölgelerindeki sertliği değerlendirmek için "PROCEQ Equotip Bambino 2 Portable" Sertlik test cihazı kullanıldı. Bu cihazın çalışma prensibi, metal numuneyi etkiledikten sonra darbe gövdesindeki enerji kaybındaki sertliği elde etmektir. Her bölge için, 3 farklı nokta sertliği ölçülmüş ve ortalamaları bu bölgenin sertliği olarak beyan edilmiştir. Çekme mukavemeti testi için, gerilme testi numuneleri, her iki ardışık kaynak bölgesini içeren boruların enine kesitinden kesilmiştir. Çekme Testleri, bir "ASLA Üniversal Çekme Test" Makinesi kullanılarak oda sıcaklığında yapılmıştır. Charpy darbe testi için, numuneler ITAB'ın ortadaki boruların üst üste binen kısmından ve diğer taraftan ITAB kaynak merkezinden uzaklığı ile kesildi. Malzemenin kırılgan davranışını incelemek için tüm numuneler sıvı nitrojen içinde tutuldu. Her bölge için üç çarpışma testi örneği sağlandı.

Sertlik testine göre, en fazla sertlik iki ITAB'n üst üste geldiği bölgede alınmıştır. Bu bölgede sertlik boruların kalınlaştikca, paso sayısının artmasiyle daha fazala bir miktarda oluyor. normalde ITAB bölgelin sertliği kaynak merkezinden uzaklaştıkca duşmesi gerekiyor ama, ITABlarin üst üste geldiği durumda, dış bölgede oluşan çevresel artik gerilmelerin artmasi sebebiyle, sertliğin azalmadığı hatta küçük bir miktarda başka kısımların sertliğine göre daha fazla olması tespit edilmiştir. Nemunelerin hepsi, 2 inç sch numarasi 40 olan hariç, ITAB'ların üst üste gelen bölgeden kopmuşlar. Eksenel çekme artık gerilmenin oluşması, çekme testinde ortaya çıkan uzama miktarını azaltmaktadır. Bu bölgede bu gerilmelerin üst üst gelmesiyle baraber artması, kırılmaya sebep olduğu düşünülmektedir. 2 inç 40 schedule numarada olan nemunede kırılma ıkıncı yapılan kaynağın, ITAB'nda oluşmuştur, nemuneni inceledikten sonara, iki borunun kaynak yapıldığında eksenleri aynı seviyede olmadığı tespit edildi, kirilma sebebide bu olduğu düşünülüyor. çentik darbe testi sonuçlarına bakıldığında, kırılgan tokuluğunda bu bölgede küçük bir düşüş olduğu öne çıkıyor. Kromun varlığı paslanmaz çeliğin korozyona karşı direncini artırmakta önemli bir rol oynamaktadır, Ancak ITAB'da yüksek sıcaklıklarda, Tane sınırlarında Chromium Carbid'in çökelmesi nedeniyle HAZ'da yüksek sertlik değerlerine neden olur ve bu fazın kırılgan davranışından dolayı paslanmaz çeliklerin mekanik özelliklerinde azalma olur. Baz metallere yaklaşılarak, kaynak sıcaklığında azalma nedeniyle, tokluk ve mekanik özellikler genellikle geri kazanılır. Ancak, yoğun kaynaklardaki artık gerilmeler ve tekrarlanan ısınma ve soğuma nedeniyle yakın kaynaklarda, HAZ'ın kırılgan sertliği azalır.

Bu çalışmada, ABAQUS yazılımı ile 304L (östenitik paslanmaz çelik) boruların çok passolu TIG kaynağını simüle etmek için bir uc boyutlu Sonlu eleman modeli geliştirilmiştir. Bu süreç, borular üzerindeki kaynak etkilerini gözden geçirmemize ve uzunluğunu belirlememize olanak sağlar. sayısal yönteme ve deneysel testlere dayanarak, Çok yakın kaynakların arısında kalan borularda mekanik özelliklerinde bir düşüş tespit edilmiştir Bu borular işe alındığı takdirde, farklı kayıplara yol aça bilmek potansiyeline sahiptirler. Iki kaynağın ITAB'larının üste üste gelmesiyle berabar bu bölgelerde oluşan artık gerilmeller üst üst geliyor ve bunun sonucu olarak malzemenin mekanik özelliklerinde bir düşüş oluyor. Sonuca bakarak, ITAB'ların üst üste gelmasi istenen bir durum olmadığı ve bunu önlemek için, iki kaynak arasında ki mesafenin ITAB'ın iki katinan daha uzun olması gerektiğin bu çalışmada öne çıkmıştır.

1. INTRODUCTION

1.1 Definition of Problem

Pipes and piping components play a crucial role in power plants, refineries and upstream/downstream energy transmissions. Since Pipes are manufactured in standard sizes and lengths, a joining approach is required to achieve desired system designs. Arc welding as a reliable and efficient metal joining process is used to join pipes. The method of welding applied to circumferentially join two pipes depends on the magnitude of outer diameter and wall thickness of pipes. For joining pipes with small outer diameters (upto 4″) Tungsten Inert Gas (TIG) welding is mostly used. As a result of intensive temperature cycles of arc welding, changes in the microstructure and mechanical properties of some regions of base metal is an undeniable effect of welding. The most influenced region of base metal is called as Heat Affected Zone (HAZ). In power plants and refineries, due to complex system designs and fittings, in some lines, the distance between two circumferentially welded joints, as shown in figure 1.1, is relatively too much small. In service conditions that pipes are subjected to high pressure and temperature rates, leakages are reported in these parts.

Figure 1.1: two close welds **[1]**

It seems to be the effect of overlapping of two close welds' HAZs, which can influence the mechanical behavior and microstructure of pipes. There is no standard for the minimum distance between two consecutive welds in literature and references.

1.2 Purpose of Thesis

In this study, effects of overlapping of two consecutive close welds' HAZs on the mechanical properties of pipes were investigated. The effect of inconstant heating and cooling in this regions and generated residual stresses as a result of temperature cycles were studied and their influence on the mechanical properties of material was aimed to be revealed. In this study, four austenitic stainless steel (304L) pipes with different outer diameters and wall thicknesses were analyzed for this situation. At the first stage, finite element analyses are carried out for simulation of the pipes' multipass TIG welding in order to study the effect of welding on the HAZs and identified the lengths of HAZs generated on four different pipes due to intensive heating. Then considering these values, a real model was created to develop a situation in which two consecutive HAZs are overlapping. In the next step, experiments are done to investigate mechanical properties of pipes in HAZ overlapping situation. And finally, for the analyzed pipes, the minimum distance between welds is established to minimize the defects and leakages in practical applications.

2. FUNDAMENTALS

2.1 Tungsten Inert Gas Welding (TIG)

Welding is a fabrication method in which two or more pieces of metal are joined together by application of heat, pressure or a combination of both. In a general classification, welding processes can be specified in two groups:

1. Pressure welding: Weld is achieved by means of pressure.

2. Heat welding: Weld is achieved by means of heat.

Heat welding processes are widely used in different parts of industry today. Among the methods of heat welding, Arc welding is one of the most important approaches used for joining of structural elements for a wide range of applications such as nuclear reactor, automobile, pressure vessels, refinery pipelines and etc.

In Arc Welding, a continues supply of either direct or altering electric current is used to establish an electric arc which delivers enough heat energy to melt the base metal and form a weld. Since the high temperature fields generated during welding, there may be severe distortions and high levels of residual stresses which leads to reduction in strength and results in different types of failure. Hence, arc welding is a very complex process and it requires careful considerations.

The most common types of arc welding include:

- Shielded Metal Arc Welding (SMAW),
- Gas Tungsten Arc Welding (GTAW) or Tungsten Inert Gas(TIG)
- Gas Metal Arc Welding (GMAW),
- Submerged Metal Arc Welding (SAW).

The original objective of any welding process is to get a weld with similar properties to the base metal. The way to obtain such a weld is to protect the molten puddle from

the atmosphere. In gas shielded-arc welding, this protection is done by application of an inert gas. This inert gas prevents the atmosphere from contaminating the weld.

Gas Tungsten Arc Welding (GTAW) or Tungsten Inert Gas (TIG) welding is a type of shielded metal arc welding. In this process, metals are melting and joining by heating them with an arc occurred between a non-consumable tungsten electrode and the metals, and the weld zone are surrounded by an inert gas (i.e. either helium or argon or a mixture of the two as usual) that eliminates the possibility of weld contamination by the atmosphere [1].

The overall process and enlarged TIG welding area is shown in figure 2.1.

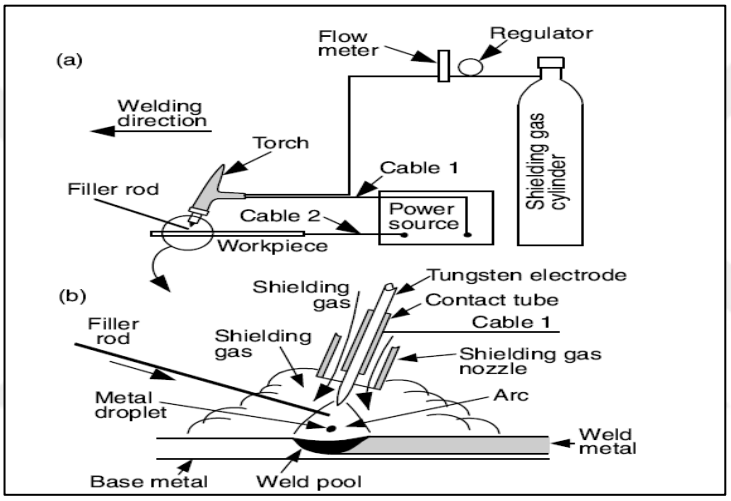

Figure 2.1: TIG Welding equipments and process **[1]**.

2.1.1 Polarity in GTAW

Three different types of polarity (shown in figure 2.2) are applied in GTAW welding.

- **Direct Current Electrode Negative (DCEN):** in this approach (also called straight polarity), electrode is connected to negative terminal of the power supply. Hence electrons will be emitted and accelerated from electrode to the workpiece thus more power will be in workpiece. This type of polarity is applied for thick materials for achieving narrow and deep welds.
- **Direct Current Electrode Positive (DCPN):** in this case (known as reverse polarity), heating effect of electrons will be higher in electrode and it leads to a shallow weld.in reverse polarity, positive ions of shielding gas bombard the workpiece. Consequently, oxide layers are broken and final surface will be smoother.

- **Altering Current (AC):** a combination of good penetration and oxide cleaning can be achieved. AC is usually applied in joining aluminum parts.

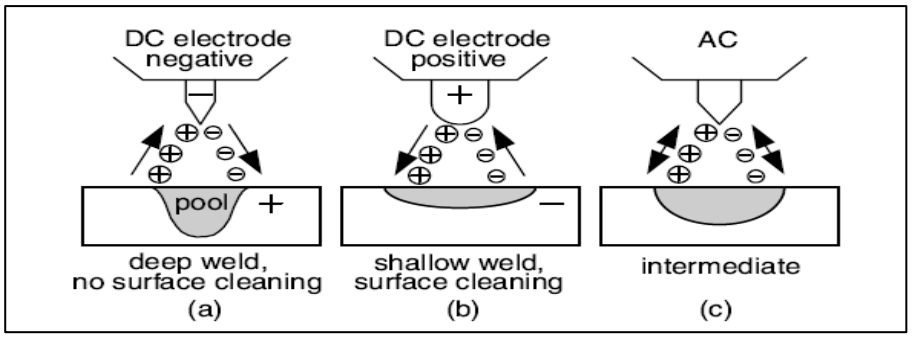

Figure 2.2: different types of polarity in TIG welding **[1]**.

2.1.2 Shielding gasses in GTAW

The primary task of a shielding gas is to protect the weld pool from the influence of the atmosphere, i.e. from oxidation and nitrogen absorption, and to stabilize the electric arc. The choice of shielding gas can also influence the characteristics of the weld penetration profile [2]. The normal gas for TIG welding is argon (Ar). Helium (He) can be added to increase penetration and fluidity of the weld pool. Argon or argon/helium mixtures can be used for welding all grades. In some cases, nitrogen (N_2) or hydrogen (H_2) can be added in order to achieve special properties. Table 2.1 lists the properties of shielding gasses [2].

Table 2.1: Properties of inert gasses **[2].**

GAS	Chemical Symbol	Molecular Weight (g/mol)	Specific gravity with respect to Air at 1atm and $0°C$	Density (g/L)	Ionization Potential (eV)
ARGON	Ar	39.95	1.38	1.784	15.7
Carbon dioxide	CO_2	44.01	1.53	1.978	14.4
Helium	He	4.00	0.1368	0.178	24.5
Hydrogen	H_2	2.016	0.0695	0.090	13.5
Nitrogen	N_2	28.01	0.967	1.25	14.5
Oxygen	O_2	32.00	1.105	1.43	13.2

2.1.3 Multi-pass TIG Welding

The relatively large wall thicknesses in the piping systems, the butt-weld is often constructed of several weld passes. Due to the intense concentration of heat in the welding, the regions near the weld line undergo sever thermal cycles. Multi-pass weld holds some excellent properties such as microstructural refinement, better toughness and less residual stresses compared to single pass weld. This is because [3]:

- The thermal cycle from subsequent passes refine the grains from the previous pass
- Total heat input per weld pass is reduced, therefore grain growth is effectively reduced
- Previous passes provide some preheating effect that tends to extend the critical cooling time
- The subsequent passes have an annealing effect on the previous one, thereby relieving residual stresses from the previous passes

2.1.4 Advantages and disadvantages of GTAW

In TIG welding high quality welds can be achieved due to high degree of control in heat input and filler additions separately. TIG welding can be performed in all positions and the process is useful for tube and pipe joint. The TIG welding is a highly controllable and clean process needs very little finishing or sometimes no finishing. This welding process can be used for both manual and automatic operations. The TIG welding process is extensively used in the so-called high-tech industry applications such as nuclear industry, Aircraft, Food processing industry, Maintenance and repair work, Precision manufacturing industry, Automobile industry and etc. [1]

GTAW's advantages is listed below:

- Able to join most of metals and alloys
- Welding can be done in all positions
- Comparing to other processes, free of spatter
- Produces high quality less distortion welds
- Weld can be done either with or without filler wire
- Able to join metals susceptible to oxidation like aluminum and magnesium

- Gives precise control of welding heat through pulsing
- Filler metal does not cross the arc. The amount added doesn't depend on the weld current level.
- Can be used with a range of power supplies

Limitation of this method are:

- Slow welding speed.
- Deposition rates are lower comparing to consumable arc welding.
- Requires slightly more dexterity and welder coordination than gas metal arc welding.
- Problematic in drafty environments because of difficulty in shielding the weld zone properly.
- It is not generally used for very low melting metals such as tin and lead

2.2 Heat Affected Zone (HAZ)

Figure 2.3 shows the temperature distribution during the TIG welding of a S30432 stainless steel pipe [4]. Since the high temperature fields generated during welding, , it is remarkably vital to have a clear view over the metallurgical and mechanical transformation happened in metals.

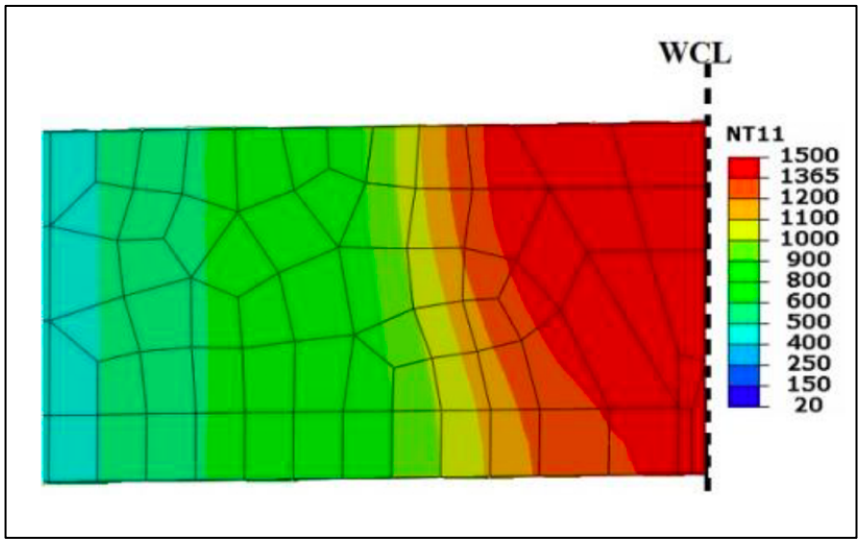

Figure 2.3: the temperature distribution during the TIG welding of a S30432 stainless steel pipe. **[4]**

Heat affected zone (HAZ) is a part of metal where the high temperature is too low to melt the part but high enough to change the microstructure and properties of the materials remarkably. The heat from the welding process and subsequent re-cooling causes this change from the weld interface to the termination of the sensitizing temperature in the base metal. As shown in Figure 2.4, the closer to the fusion zone boundary, the higher the peak temperature becomes and the longer the material stays above the effective recrystallization temperature (T_x). Under rapid heating during welding, the recrystallization temperature may increase because recrystallization requires diffusion and diffusion takes time. Since the strength of a work hardened material decreases with increasing annealing temperature and time, the strength or hardness of the HAZ decreases as the fusion boundaries approached. [1]

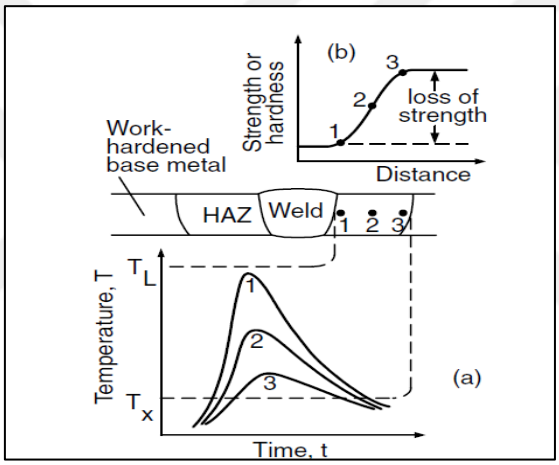

Figure 2.4: effect of Temperature cycles on hardness and strength of base metal. **[1]**

The extent and magnitude of change in this property depends primarily on the base material, the weld filler metal, and the amount and concentration of heat input by the welding process [4]. Therefore, identifying and controlling heat affected zone properties and width, makes the resultant weld joint more acceptable. HAZ width depends on different parameters explained in next chapters.

There are different sub-zones in HAZ microstructure due to altering thermal cycles experienced in different zones of HAZ. The HAZ microstructure of the welded joint of a low-alloy steel is shown in Figure 2.5. Since increasing in temperature leads to increase in grain growth, the grain size in HAZ increases as the fusion boundary approaches.

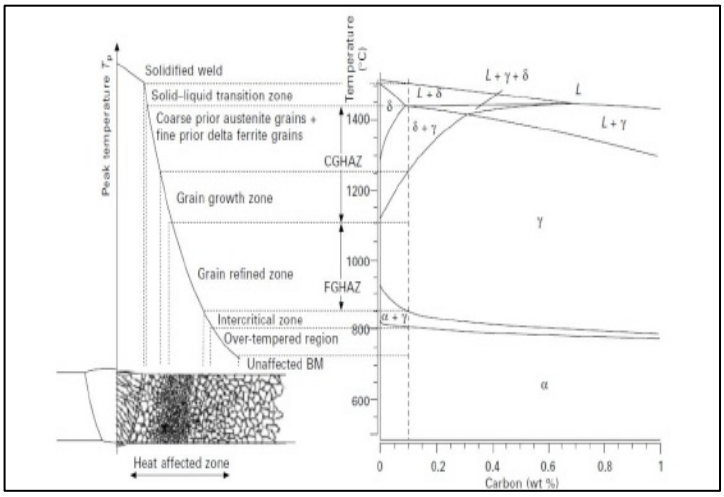

Figure 2.5: Schematic of the sub-zones of the HAZ corresponding to the calculated equilibrium phase diagram of P91-type steel. **[5]**

2.2.1 HAZ sub-zones in single pass welding

These sub-zones are frequently described by abbreviations shown in Figure 2.5, taken from [5].These abbreviations are explained in Table2.2

Table 2.2: HAZ sub-zones in single pass welding. **[5]**

Zone	Definition	Maximum temperature
CGHAZ	Coarse Grain Heat Affected Zone	$A_3 \leq T_m \leq T_{Melting}$
FGHAZ	Fine Grain Heat Affected Zone	$A_2 \leq T_m \leq A_3$
ICHAZ	Inter Critical Grain Heat Affected Zone	$A_1 \leq T_m \leq A_2$
SCHAZ	Sub Critical Heat Affected Zone	$T_n \leq T_m \leq A_1$

The balance of strength and toughness in the weld heat affected zone (HAZ) is usually upset due to the effect of welding thermal cycles.

The research [6] is focused on mechanical properties and microstructure of CGHAZ of ASTM4130 steel prior and after post welding heat treatment(PWHT). It shows that the impact toughness in CGHAZ of ASTM4130 steel is only 5.5%–7.1% that of the base metal, which makes CGHAZ become the local brittle zone in single-pass welding. It also declares that width and toughness of CGHAZ is highly depends on the heat input in welding process.

The authors in [7] analyzed microstructure and mechanical properties of FGHAZ of ASTM 4130 steel. The results show that serious embrittlement occurs in the FGHAZ with an 81.37% decrease of toughness, compared with that of the base metal due to microstructural transformation occurred in material as a result of thermal cycles

2.2.2 HAZ subzones in multi-pass welding

As it is told before,Welding of thick steel structural elements usually requires the application of a multi-pass welding procedure. The thermal cycles of multi-pass welds have a significant influence on the mechanical and the metallurgical properties of the welded joints. In a multi-pass weld, the HAZ from the former bead overlaps the HAZ from the latter one and consequently a variety of partially and fully reheated zones will be created. Different zones of a two-pass welding are shown in Figure2.6. In this case, the first pass (weld pass 1) HAZ regions are reheated to different peak temperatures during the second weld pass thermal cycle (weld pass 2).

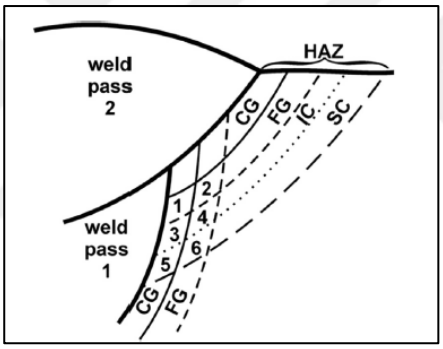

Figure 2.6: Schematic of the sub-zones of the HAZ in two pass welding

Table 2.3: two pass welding HAZ subzones definition

zone	abbreviation	Open form
1	SCR CG HAZ	Super-Critically Reheated Coarse-Grain Heat Affected Zone
2	IR CG HAZ	Inter-Critically Reheated Coarse-Grain Heat Affected Zone
3	SC CG HAZ	Sub-Critically Reheated Coarse-Grain Heat Affected Zone
4	SCR FG HAZ	Super-Critically Reheated Fine-Grain Heat Affected Zone
5	IR FG HAZ	Inter-Critically Reheated Fine-Grain Heat Affected Zone
6	SC FG HAZ	Sub-Critically Reheated Fine-Grain Heat Affected Zone

The zones of most importance are the sub-critically and inter critically reheated coarse-grained HAZ regions, in which the previous microstructure is either tempered or partially retransformed and re-cooled. In this Zones because of microstructural transformations weld joints toughness decreases remarkably [8].

2.3 Parameters Controlling Heat Affected Zone Width and Properties

The size and properties of HAZ (and its subzones) depend on many factors such as properties of base metal, parts thickness, welding process performed, welding time, maximum temperature, value of linear electric energy of welding arc, welding conditions, cooling efficiency, type of weld filler metal, heat input and the others [10]. The most important factors are explained below.

2.3.1 Material welded

Welding a material with high Thermal diffusivity results in a narrow HAZ because of high cooling rate and by decreasing thermal diffusivity, cooling rate decreases and leads to a wider HAZ area. As shown in the following formula, Thermal diffusivity (α) is a function of materials density (ρ), thermal conductivity (k) and specific heat capacity (c_p).

$$\boldsymbol{\alpha = \frac{k}{\rho c_p}} \tag{2.1}$$

The changes in the HAZ are also dependent upon the prior thermal and mechanical history of the material. For example, the recrystallization behavior during the heating cycle is affected by whether the original material was in cold rolled or annealed condition prior to welding.

2.3.2 Thickness and cooling rate

The size of part in welding would greatly affects cooling rates. Thick joints lead to fast cooling rates of the weld zone due to the large contact area and consequent rapid heat flow to the surroundings, while thin joints lead to a relatively slower cooling rate. A slow cooling rate results in forming a low toughness microstructure while a fast cooling rate makes the structure more brittle [11].

Hardness also changes by changing thickness. In [9] researchers investigated the effect of thickness in the hardness of resulted joint fabricated by application of shield metal arc welding. Experiments show that hardness increases with thickness increasing. It can be explained by finer grain sizes resulted in fast cooling rates.

2.3.3 Heat input and maximum temperature

Among the various parameters of the welding procedure, heat input (Q) is the most important variable needed to be controlled, as it incorporates the welding voltage (V), the current (I) and the torch travel speed (s) as shown in equation (2.2)

$$\mathbf{Q = \mu \frac{VI}{s}} \tag{2.2}$$

As shown in Figure 2.7 Heat input has a remarkably large effect on the size and properties of heat affected zone. By increasing in heat input per length of weld the width and the retention time above the effective temperature (recrystallization temperature) increases [1].

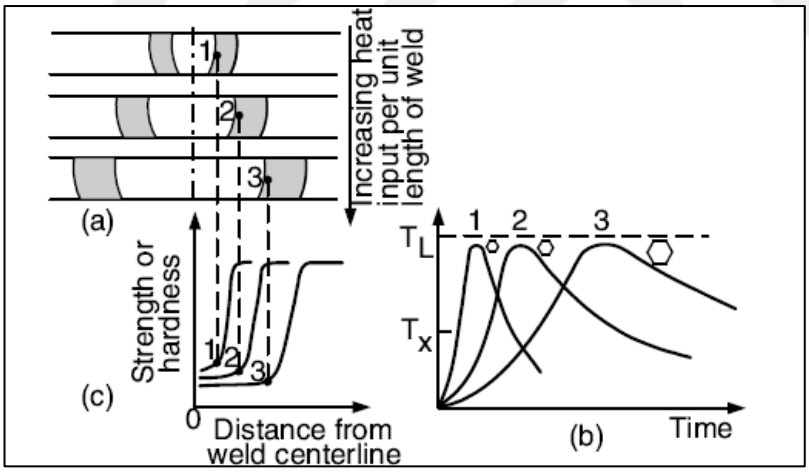

Figure 2.7: effect of input on HAZ properties**. [1]**

In [10] a research was carried out to understand the heat transfer behavior during TIG welding of pipes by using finite element heat transfer analysis. The peak temperature of the welding analysis was varied between 1600°C and 2600°C. It is observed that the peak temperature at higher heat input was very high as the convection effects of weld pool was neglected during the simulation.

In [11] investigations on the effect of welding parameters final HAZ size decproperties declared that Among the welding parameters, the welding current has the greatest influence on HAZ size.

Furthermore, multipass welding increases the complexity of both the thermal and the microstructure transformation phenomena because the metal is subjected to multiple repeated thermal cycles. The Authors in [12] investigates the influence of low and high inputs for multipass welding of High Strength Low Alloyed (HSLA) steels. The results show that a 9-pass welded joint with low heat input is stronger than a weld performed in 7-pass but in high heat input.

2.4 Austenitic stainless-steel pipes

Stainless steels pipes are widely utilized in different aspects of industry such as food, petrochemicals and electric power industries. In particular, austenitic stainless steels are commonly applied due to their excellent combination of mechanical properties and resistance to corrosion. This is as a result of its alloy components where high chromium content leads to the formation of a dense passivation layer, increasing corrosion resistance at high temperatures. Extitance of nickel and manganese causes to stabilize the austenitic phase for its mechanical properties, namely high-temperature ductility and creep resistance [13].The low content of carbon avoids the formation of chromium carbides which lead to embrittlement and sensitization. The silicon is added to the alloy to elevate corrosion resistance, especially at high temperatures. The combination of silicon and chromium provide superior corrosion resistance without high susceptibility to creep [13] .

In this study, Austenitic stainless steel 304L is the material to be investigated. AISI 304L steel has a reduced carbon content of 0.035 wt.% or lower which restricts the precipitation of carbides, making it suitable for welding and for use in power plant applications, where gases and air at high temperatures need to be transported to and from functional parts such as boilers and turbines [13]. Existance of Chromium plays a significant role in increasing the resistance of stainless steel against corrosion, but in high temperatures in HAZ, because of Chromium precipitation as Chromium Carbid in grain boundries results in high hardness values in HAZ and decreases in mechanical properties of stainless steels due to brittle behavour of this phase [14].

In the table2.4 information about chemical composition.

Table 2.4: Chemical composition of Austenitic stainless stell304L. **[13]**

Grade	C	Mn	P	S	Si	Cr	Ni
304L	0.03	2.00	0.045	0.030	1.00	18-20	8-11

According to phase diagram, the approximate microstructure during welding of a 304L alloy is shown in figure 2.8. it is clear that by reaching to the 550℃ the microstructure change starts in the base metal and in the 1400℃ the steel begins to melting. hence the HAZ temperature range for austenitic stainless steel 304L includes temperatures between 550℃ and 1400℃.

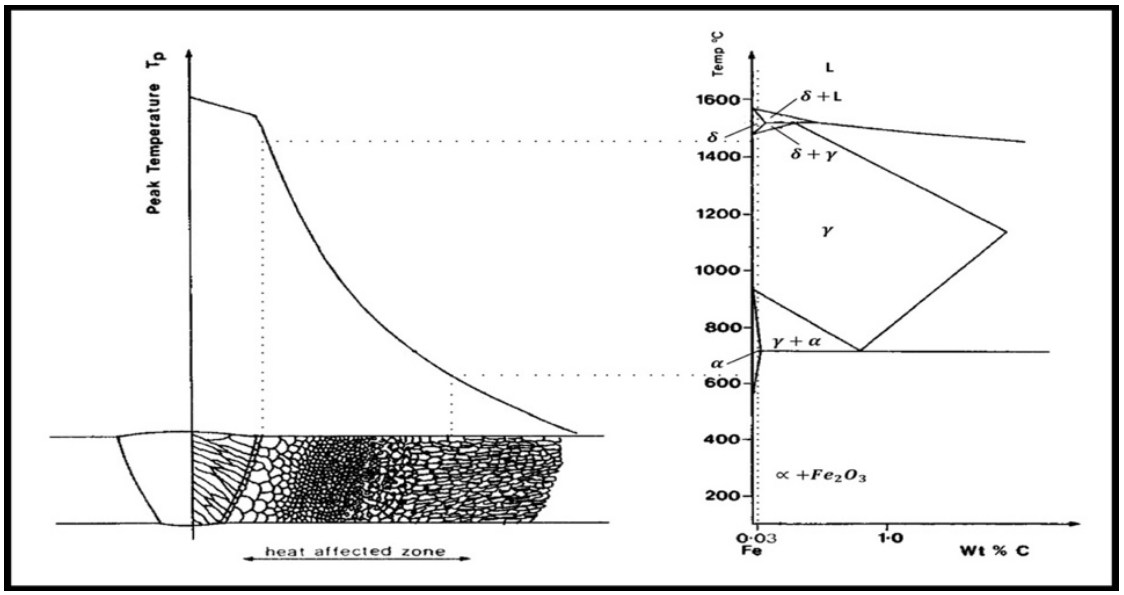

Figure 2.8: schematic diagram of the various sub-zones of the heat-affected zone approximately corresponding to the alloy (0.03 wt% Carbon) indicated on the Fe-Fe3C equilibrium diagram.

3. WELDING FINITE ELEMNENT ANALYZING

3.1 Introduction

Fusion Welding is the main metal joining process in many manufacturing industries. For welding stainless steel piping systems, the circumferential butt-weld is the main applied process. Owing to the relatively large wall thickness in such piping systems, the butt-weld is mostly performed in several welding passes in order to join relatively thick pipes. As a result of the intense concentration of heat in the welding, the parts of pipes near the weld line are exposed to sever thermal cycles which may cause non-uniform heating and cooling in the material, thus generating inhomogeneous plastic deformation and residual stresses in the weldment [15]. The presence of residual stresses can be detrimental to the performance of the welded product. The strength and quality of welding is completely related to the resultant microstructure of weld pool and heat-affected zone. HAZ properties and microstructure are directly controlled by the heat transfer rate during welding. Therefore, a good estimation of the welding temperature and residual stress fields is then needed. Predicting the weld quality in the means of modeling the heat transfer is a topic of interest to both researchers and industrialist for the last few decades. For modeling of heat transfer during welding, different numerical and analytical methods have been applied by different authors and they have their own advantages and limitations. At present, commercial FEM software's are commonly used for solving.

The research [15] reviews the studies in the area of arc welding heat transfer simulation. Starting from fundamentals of arc physics, heat transfer, microstructure models, thermal stress, and modern techniques like pattern recognition comes into picture while considering the complete solution of welding-related problems.

Over the last decades, Simulation of circumferential welding through finite element method is the topic of many researchers. The authors in [16-18] have employed the rotational symmetry condition (axisymmetric condition) in order to reduce

computational power requirements and time. The axisymmetric approach can decrease the computational time and procedure but make the simulation over simplified by restricting the analysis to only one part of the complete geometry. According to this research, the results obtained tend to reflect the residual stress distribution in circumferentially welded pipe in an average sense and cannot be interpreted, strictly speaking, as a representation of a cross section away from the welding start/stop positions.

The authors in [19] investigates the temperature cycles and residual stress fields in a single pass TIG welding of a SUS304 stainless steel by the means of a 3D FE model. Then based on results of this simulation, a 3D elasto-plastic FE model is developed to study the stress distribution under superimposed mechanical axial tension in the welded pipe. The results show that both the traveling arc and welding start\stop effects tend to violate the axisymmetric assumption, therefore, a 3D model is essential for analyzes.

In the research [20], 3D and 2D models are developed to simulate the multipass welding in SUS304 stainless steel pipe in the means of FEM. Both results obtained by 3D and 2D models are in good agreement with experimental results but 3D simulation leads to more accurate results in a relatively long computational time where 2D analyzes produced less precise results in a short computational time.

The authors in [21] make an effort to apply an adaptive meshing technique combined with a suitable data transfer method to simulate 13-pass TIG welding of 316L stainless steel pipes. This method reduced the requirement for a powerful computer and long times of computation but comparing to other methods, the results are less accurate.

In the research [22] a comparison is done between the FEA results obtained from ABAQUS and ANSYS software's. Both results are in good agreement with experimental results.

In the research [10] a 3D FE analyze is carried out to predict the heat transfer behavior during a single pass TIG welding of 304L stainless steel pipes in different heat inputs. In this study effects of weld pool are neglected.it is shown that by increasing heat input, there is a increase in peak temperature in base metal.

The authors in [23] effort to develop a 3D model for a multipass TIG welding of SUS304 stainless steel and investigate the temperature fields and residual stress

distributions resulted by welding. Comparing to experimental results, it is shown that 3D finite element analyzing is a reliable and secure process to predict welding behavior and effects.

In this study, in the first step, a 3D finite element analyze is carried out for the multipass welding of each pipe to obtain temperature cycles in order to predict the magnitude of HAZ. Also, residual stress distribution in both axial and hoop direction is shown to have an understanding of thermal stresses after welding.

Practically welding process is a coupled thermo-mechanical phenomenon (figure3.1) However, since the mechanical work (residual stress field) is strongly dependent on the temperature field with negligible inverse dependency, uncoupled analysis works very well. [24]. In other words, the heat generated by mechanical work has a marginal influence on the temperature cycles during the welding process. The analyze procedure can be departed into two steps. First, the temperature distribution and its history in the welding model is computed by the heat conduction analysis. Then, the temperature history is employed as a thermal load in the subsequent mechanical elastic plastic calculation of the residual stress field.

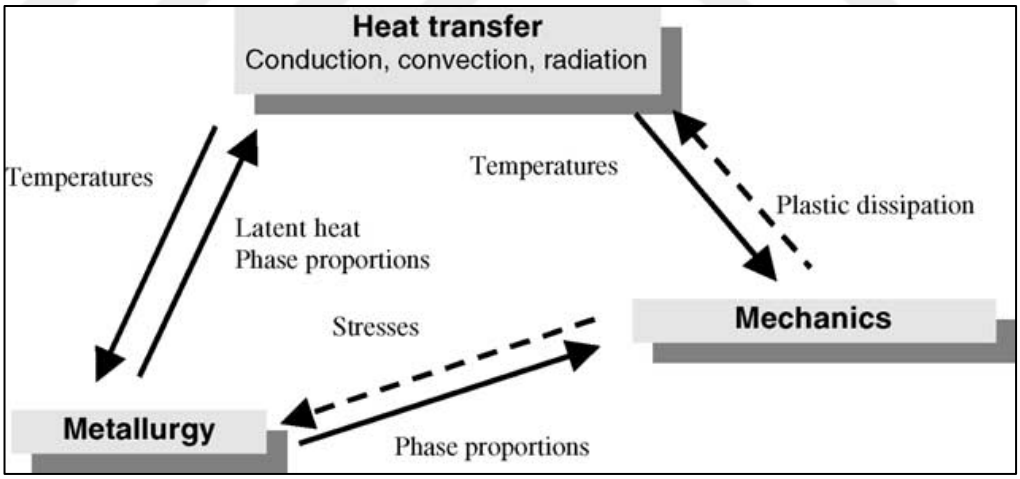

Figure 3.1: Physical phenomena involved and their couplings **[21].**

3.2 Physical Modeling and mesh generation

In this investigation four different pipes with different outer diameters and wall thicknesses undergo multipass butt TIG welding. The number of passes for welding of each pipe depends on the thickness of the respective pipe's wall thickness. The welding is carried out for all of pipes and the induced transient temperature fields and residual stresses were analyzed. The material used was considered as 304l austenitic stainless steel that does not undergo solid state phase transformation during melting and solidification.

All the pipes were meshed with hexahedron linear elements in order to obtain more precise results for analyzing the field variables. Due to the high temperature and stress gradients in the zones closer to weld center, the mesh size is finer in these regions. Element size increases progressively with distance from the weld centerline (Figure 3.2).

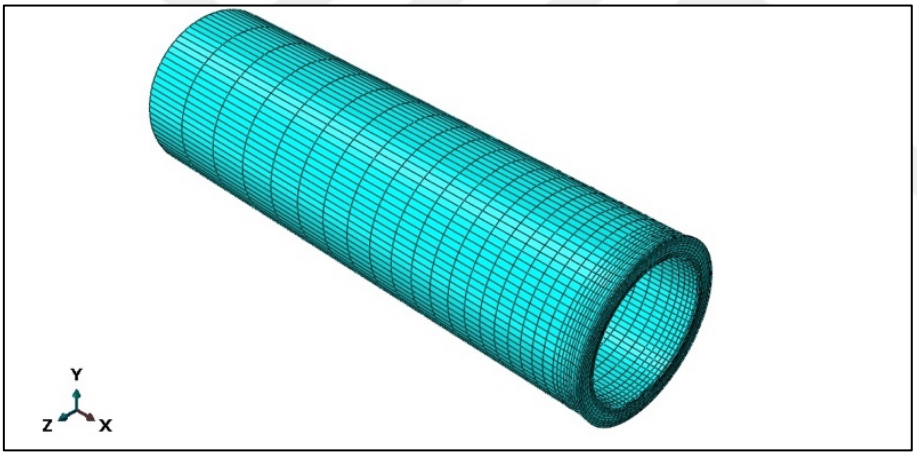

Figure 3.2: meshed model.

Each pipe is welded to the same pipe size of itself with a certain number of passes considering its thickness. The groove angle for all the samples is assumed to be 30°. The detailed information about geometric models, number of passes and nodes are given in table 2.1. The model is assumed as symmetric and one pipe is modeled in the analysis. The meshed pipe model given in the Figure3.2, is mirrored to get an understanding of the pipe welding. (Figure3.3).

Table 3.1: Geometrical information of pipes

Pipe no.	Diameter nominal	Schedule NO.	Wall thickness (mm)	Number of Welded Passes	Number of nodes-elements
1	60.3	40s	3.91	2	14960
2	60.3	80s	5.54	3	16160
3	114.3	40s	8.56	4	20640
4	114.3	120s1	11.83	6	22916

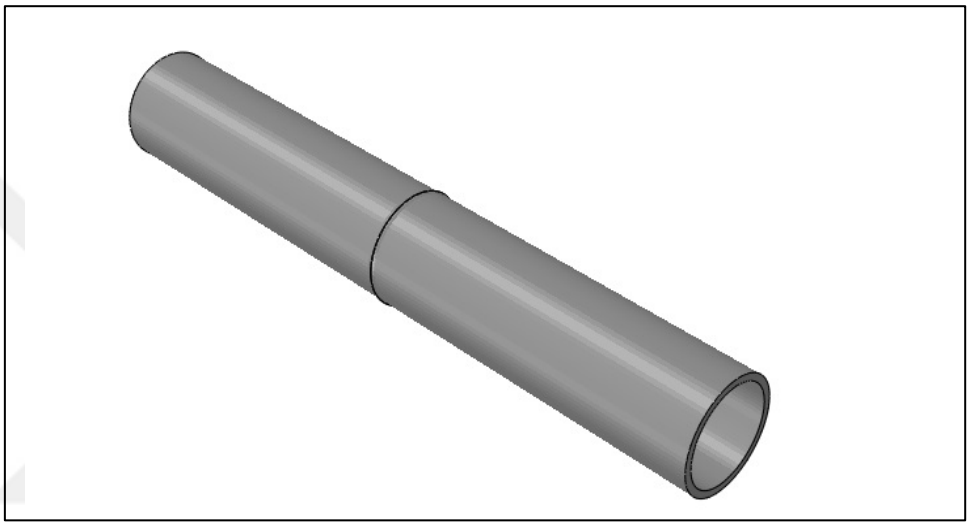

Figure 3.3: Mirrored Model.

3.3 Material Properties

The material is considered as 304L austenitic stainless steel. The temperature dependent thermal and mechanical properties of material are shown in table 2.2. These temperature dependent properties lead to non-linearity in the problem. The base metal and weld metal properties are almost the same but there is a difference in yield stress which is higher for weld metal.

Table 3.2: Mechanical and Thermal Properties of Austenitic Stainless Steel 304L.

Temperature (°C)	Specific Heat ($\frac{J}{Kg°C}$)	Conductivity ($\frac{J}{m°Cs}$)	Density ($\frac{Kg}{m^3}$)	Yield Stress (MPa)	Thermal Expansion ($10^{-5}°C^{-1}$)	Young's modulus (GPa)	Poisson's ratio
0	462	14.6	0.790	265	1.70	198.5	0.294
100	496	15.1	0.785	218	1.74	193	0.295
200	512	16.1	0.780	186	1.80	185	0.301
300	525	17.9	0.779	170	1.86	176	0.310
400	540	18	0.778	155	1.91	167	0.318
600	577	20.8	0.775	149	1.96	159	0.326
800	604	23.9	0.770	91	2.02	151	0.333
1200	676	32.2	0.768	25	2.07	60	0.339
1300	692	33.7	0.767	21	2.11	20	0.342
1500	700	70	0.765	10	2.16	10	0.388

3.4 Thermal Analysis

During the thermal analysis the model change option is used to simulate the weld metal deposition. During the first weld pass, the second weld pass does not exist in the model. After the completion of the first welding, new elements are added to the model to simulate the weld metal deposition into the groove during the second welding. This procedure is repeated for all passes. Between each two passes there is cooling step in order to reach 25°C inter-pass temperature. Since the pipes are symmetrical, half of the pipe is only modeled. In this study, all analyses are performed using ABAQUS code.

3.4.1 Governing equation

Heat Transfer in welding process is a transient heat transfer case, then time dependent heat transfer equation is the governing equation in thermal analyzing of welding. It is given by:

$$\rho c \frac{\partial T}{\partial t}(x, y, z, t) = -\nabla \vec{q}(x, y, z, t) + Q(x, y, z, t) \quad \textbf{(3.1)}$$

Where ρ and c are respectively temperature dependent density and specific heat capacity of the material, T is the temperature in any desired location and time in the pipe, t is the time, $Q(x,y,z,t)$ is the internal heat generation rate , $\vec{q}(x,y,z,t)$ is heat flux vector and ∇ is the spatial gradient operator. By applying Fourier heat flux constitutive equation:

$$-\nabla\vec{q}(x,y,z,t) = -(\frac{\partial R_x}{\partial x} + \frac{\partial R_y}{\partial y} + \frac{\partial R_z}{\partial z}) \quad \textbf{(3.2)}$$

Where:

$$R_x = -k_x \frac{\partial T}{\partial x} \quad \textbf{(3.3)}$$

$$R_y = -k_y \frac{\partial T}{\partial y} \quad \textbf{(3.4)}$$

$$R_z = -k_z \frac{\partial T}{\partial z} \quad \textbf{(3.5)}$$

Where k_x, k_y and k_z are temperature dependent thermal conductivity in respectively x, y and z directions. All these temperature dependent parameters induce non-linearity in heat transfer equations in welding.

3.4.2 Heat input condition

The temperature distribution during the welding process is a result of the heat input of the welding arc, conduction of heat through the material, surface heat losses and the thermal properties of the material.

In this study, the heat from the moving welding arc is applied as a volumetric heat source with a double ellipsoidal distribution proposed by Goldak et al. [25](figure3.4) and is expressed by the following equations:

For the front heat source:

$$q_f(x,y,z,t) = (\frac{6\sqrt{3}f_f Q}{abc_f\pi^{3/2}})e^{(-\frac{3x^2}{a^2})}e^{(-\frac{3y^2}{b^2})}e^{(-\frac{3z^2}{C_f^2})} \quad \textbf{(3.6)}$$

For the rear heat source:

$$q_r(x,y,z,t) = (\frac{6\sqrt{3}f_r Q}{abc_r\pi^{3/2}})e^{(-\frac{3x^2}{a^2})}e^{(-\frac{3y^2}{b^2})}e^{(-\frac{3z^2}{C_r^2})} \quad \textbf{(3.7)}$$

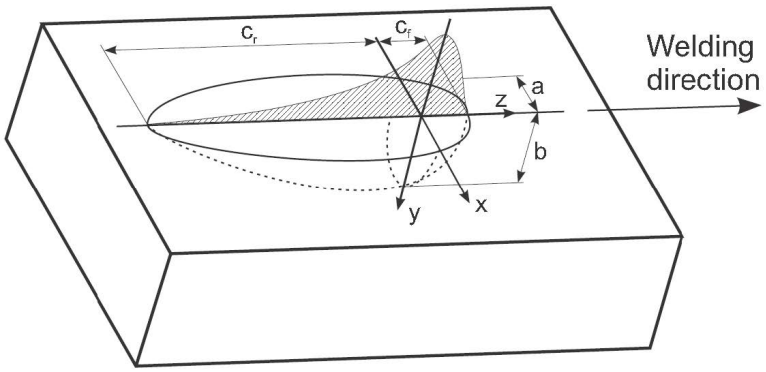

Figure 3.4: Goldak propsed heat distribution. **[25]**

Where f_f and f_r are the fraction of heat deposited in front and rear region x ,y ,z are the local coordinates of double ellipsoidal model. The parameters a, b,c_f and c_r are related to the characteristics of the welding heat source. The parameter Q is the power of the welding heat source. It can be calculated according to the welding current (I), the arc voltage (V) and the arc efficiency (η_a) by the following equation:

$$Q = \eta_a VI \quad \textbf{(3.8)}$$

Welding condition for each pass is given in the table (3-3). The arc efficiency is taken as 70% for TIG welding.

Table 3.3: Welding Condition

Pass	Current(A)	Voltage(V)	Speed (cm/min)	Heat input (kj/cm)
1	118	12	3.27	2.60
2	120	13	7.20	1.30
3	125	13.5	7.20	1.40
4	125	13.5	9.00	1.13
5	125	13.5	12.00	0.80
6	125	13.5	10.28	0.99

In this study, f_f is assumed to be 0.85 and f_r 1.15. This is done because the temperature gradient in the rear region is steeper than in the front edge. Not that $f_f+f_r=2$. [25]. The parameters of the heat source can be adjusted to create a desired melted zone according to the welding conditions. The heat source parameters assumed for a, b,c_f and c_r,are respectively 0.006,0,005, 0.005 and 0.015 According to [20]. A subroutine is generated using FORTRAN coding to apply the heat generation to the pipes. It is assumed that the pipe is welded along its circumference, and side opposite to weld line is assumed to be fixed, in order to get faster convergence during numerical analysis.

The pipes and the shapes of grooves are schematically shown in figure 3.5.

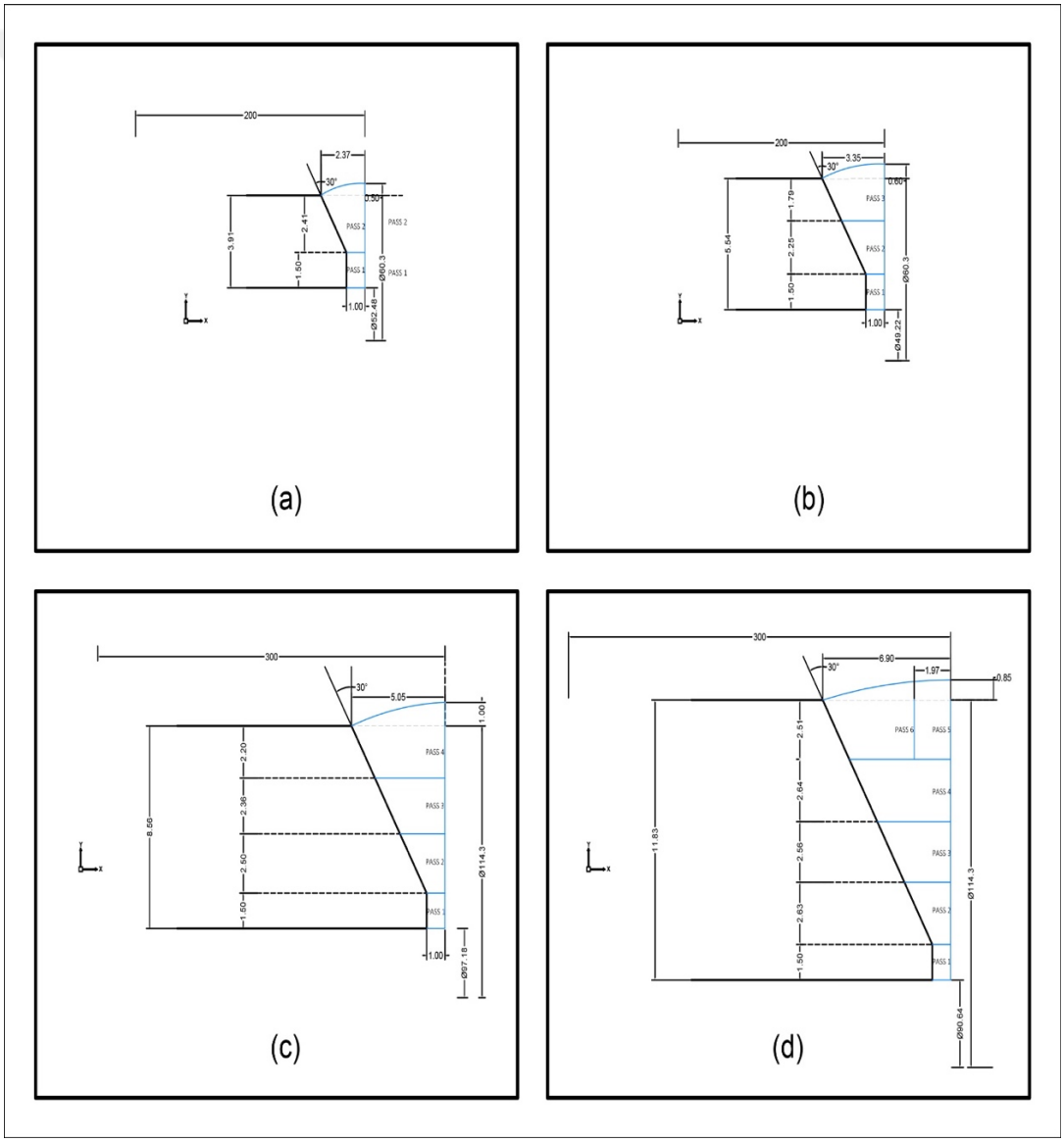

Figure 3.5: Pipes welding information: (a)PIPE Number 1, (b) PIPE Number 2, (c) Pipe number 3 and (d) Pipe number 4.

3.4.3 Boundary conditions

In this investigation, the welding process is assumed as symmetric and one pipe is modeled in the analysis. Both radiation and convection heat losses are considered all along the pipes. The axisymmetric conditions assumed mean that heat losses in the axial direction are neglected. Radiation losses plays the most dominant role for higher temperatures near the weld whereas Convection losses are important for lower temperatures some distance away from the weld, A combined boundary condition, which takes into account both radiation and convection is used in this work, An user subroutine is developed in FORTRAN and applied to simulate the combined convective and radiation boundary conditions. The combined convective and radiative heat transfer coefficient (α_h) from Dean Deng et al [20] is given as:

$$= \begin{cases} 0.68T \times 10^8 \left(\frac{W}{mm^2}\right) & 0℃ < T < 500℃ \\ (0.231T - 82.1) \times 10^{-6} \left(\frac{W}{mm^2}\right) & T \geq 500℃ \end{cases} \quad (3.9)$$

Where T is the temperature.

This thermal boundary condition is employed for all free boundaries of the pipes including the boundaries generated by the last weld passes in all the above-mentioned pipes. To account for heat, transfer due to fluid flow in the weld Pool, an artificially increased thermal conductivity, which is several times larger than the value at room temperature, is assumed for temperatures above the melting point. The thermal effects due to solidification of the weld pool are modeled by taking into account the latent heat of fusion. The initial temperature is assumed to be 25℃.

3.5 Mechanical Analysis

Mechanical analysis is carried out by the same mesh model as used in the thermal analysis. In this step analysis is conducted using the temperature histories computed by the thermal analysis as the input data. Since solid-state phase transformation does not occur in the stainless base metal and the weld metal in the duration of welding, the total strain rate can be decomposed into three components as follows:

$$\dot{\varepsilon_T} = \dot{\varepsilon_e} + \dot{\varepsilon_p} + \dot{\varepsilon_{th}} \tag{3.10}$$

Where $\dot{\varepsilon_e}$ is the elastic strain, $\dot{\varepsilon_p}$is the plastic strain and $\dot{\varepsilon_{th}}$ is the thermal strain.The elastic strain is modelled using the isotropic Hooke's low with temperature-dependent Young's modulus and Poisson's ratio and the thermal Strain is computed using the temperature dependent coefficient of thermal expansion. For the plastic strain, rate independent plastic model is employed with the following features: temperature-dependent mechanical properties and linear kinematic hardening model. Kinematic hardening is taken into account as an important feature because material points typically undergo both loading and unloading during the course of the welding process.

The FEA precdure followed in this investigation is verified in many of previous works [20-26] and the results are in good agreement with experimental works. For example, the results obtained from pipe 1, for two-pass welded 304L pipe, is compared to expermenal work done in [20].

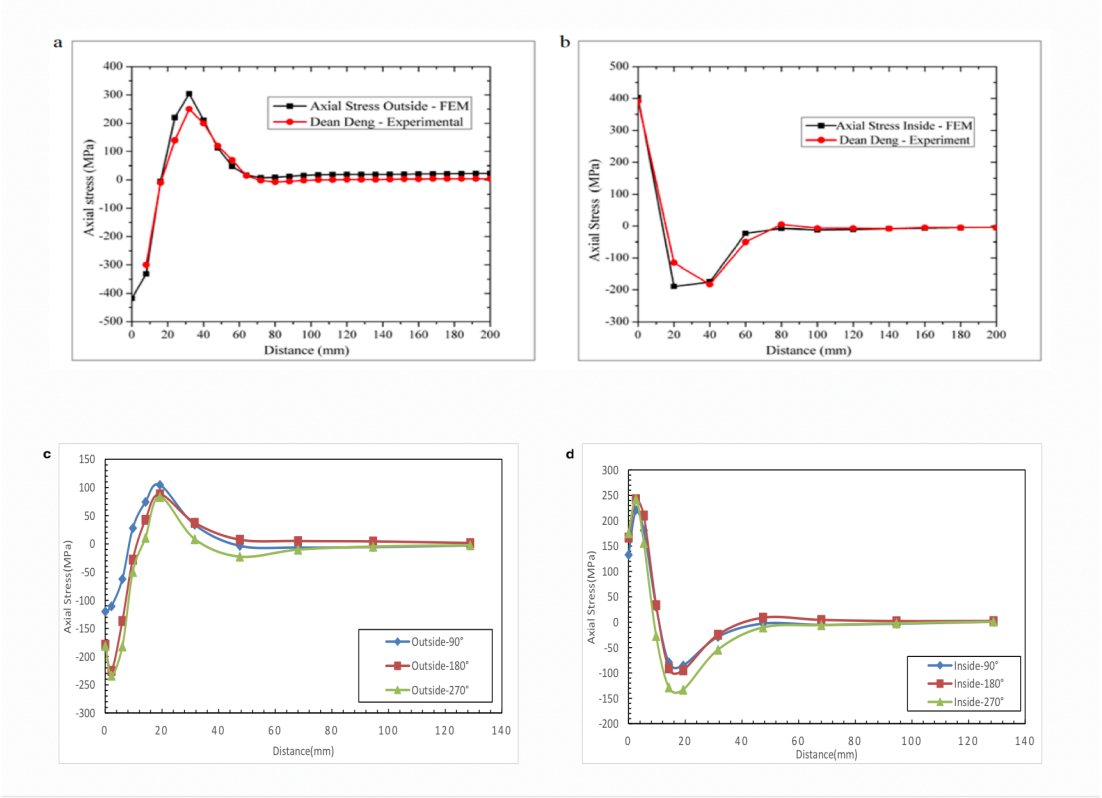

Figure 3.6: Axial stress distribution; a: outside surface obtained from **[20]** and **[23]**, b:inside surface obtained from **[20]** and **[23]**, c: outside surface results, d:inside surface results

In this investigation a two-pass TIG weld was carried out to join two 304L stainless steel pipes. The distribution of results obtained from both methods are in acceptable similarity. The diffrences attribute to variety of welding conditions and pipes physical geomtraies.

3.6 FEM Results

3.6.1 Temperature cycles

Thermal cycles for different location on the outer and inner surfaces of pipes are graphed in the figures below. It is clear that by approaching to the weld center peak temperatures for each pass increases. These results are in good agreement with practical experiences. It is very clear that the temperature histories at the different locations on the surface where θ is 90° are almost equal to those at the corresponding locations on the surface where θ is 180° or 270°.Therefore, it can be concluded that the temperature field is very steady when the welding torch moving around the pipe. The reason can be considered as low heat conduction comparing to welding speed due to relatively small conductivity. The length of base metal affected from temperature, increases by rising the thickness and number of passes. Inside surface of pipes are inflounced by the heating in first passes more than last ones and outside surfaces experienced high heatings in final passes. on the whole, outside and inside surfaces behavior are similar to each other.

The beginning of plots shows constant initial temperature as the heat source was away from the measurement point. The results show the temperature distribution during welding followed by cooling of a welded joint. In all the welding simulations the temperature attained quasi steady state and there was no fluctuation in the peak temperature. The peak temperature keeps on reducing in the transverse direction as the temperature gradient is higher near to the welding heat source. For all pipes, in each pass, the time required for reaching the peak temperature in different orientation on the pipe arenot same, it is because of the different welding speeds employed in each pass. Note that all the distances are considered from the weld center and because of the groove shape the heat distribution arenot equal in same distances on inside and outside surfaces.

3.6.1.1 Pipe number 1: Temperature cycles in inner and outer surfaces

On the inner surface for pipe 1:

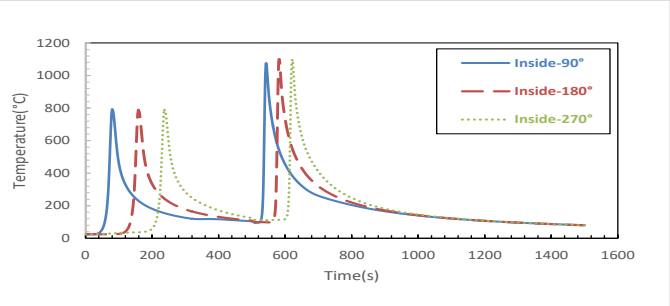

Figure 3.7: Thermal cycles at three locations on the inside surface at 2mm from the weld center for Pipe 1.

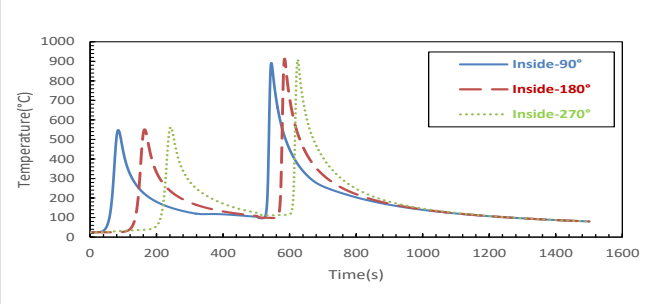

Figure 3.8: Thermal cycles at three locations on the inside surface at 4mm from the weld center for Pipe 1.

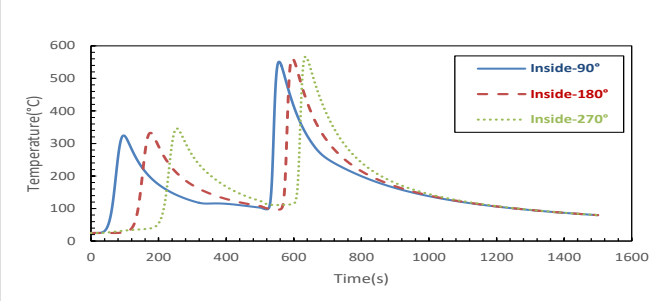

Figure 3.9: Thermal cycles at three locations on the inside surface at 10mm from the weld center for Pipe 1.

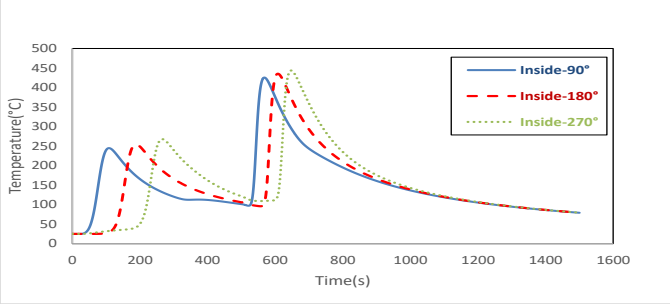

Figure 3.10: Thermal cycles at three locations on the inside surface at 20mm from the weld center for Pipe 1.

On the outside surface:

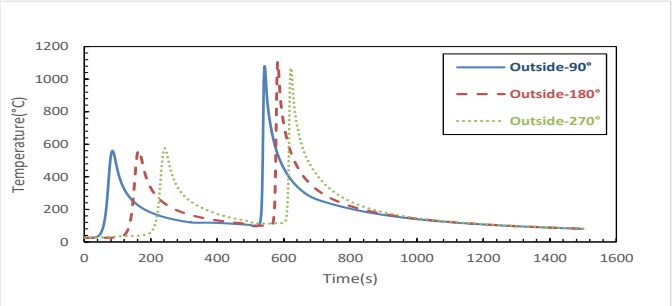

Figure 3.11: Thermal cycles at three locations on the outside surface at 3mm from the weld center for pipe 1.

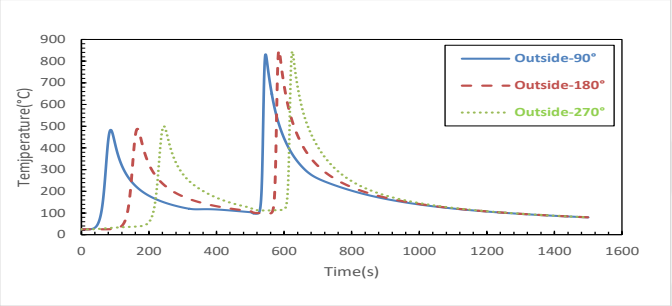

Figure 3.12: Thermal cycles at three locations on the outside surface at 5mm from the weld center for pipe 1.

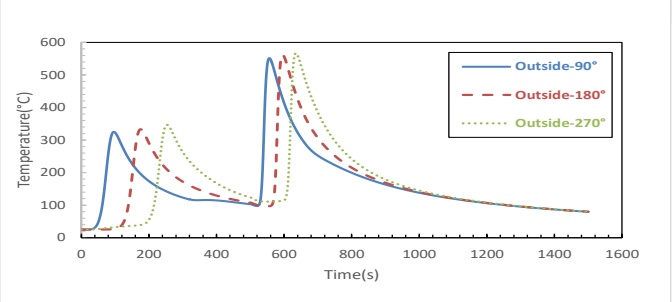

Figure 3.13: Thermal cycles at three locations on the outside surface at 10mm from the weld center for pipe 1.

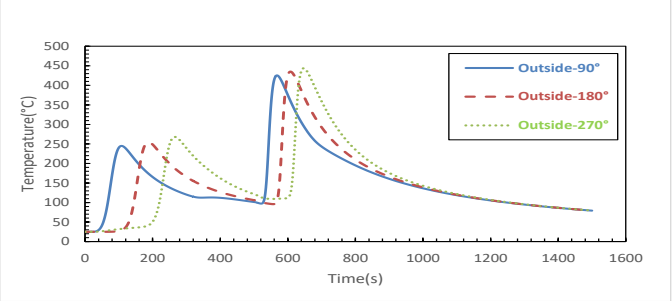

Figure 3.14: Thermal cycles at three locations on the outside surface at 15mm from the weld center for pipe 1.

3.6.1.2 Pipe number 2: Temperature cycles on inner and outer surfaces

For the pipe number 2 on the inside surface:

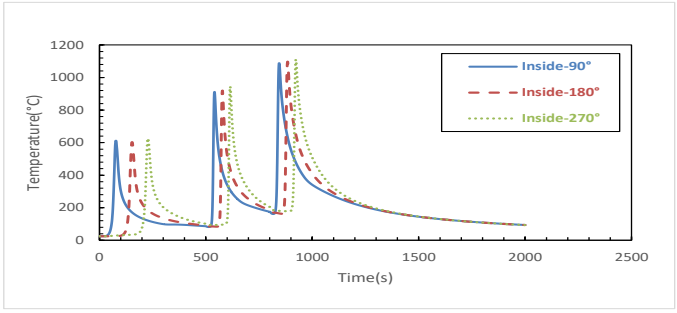

Figure 3.15: Thermal cycles at three locations on the inside surface at 2.5mm from the weld center for pipe 2.

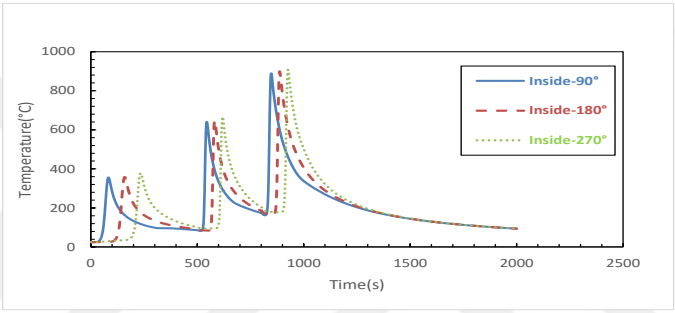

Figure 3.16: Thermal cycles at three locations on the inside surface at 5.5mm from the weld center for pipe 2

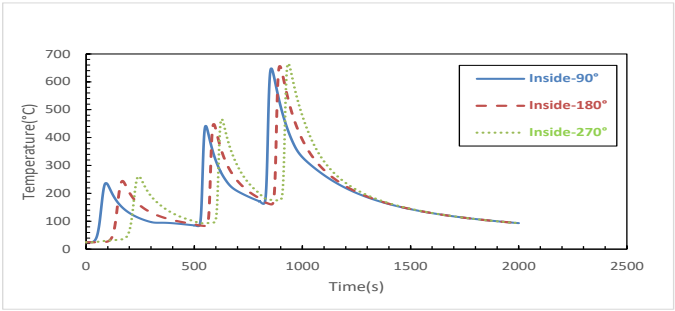

Figure 3.17: Thermal cycles at three locations on the inside surface at 10mm from the weld center for pipe 2.

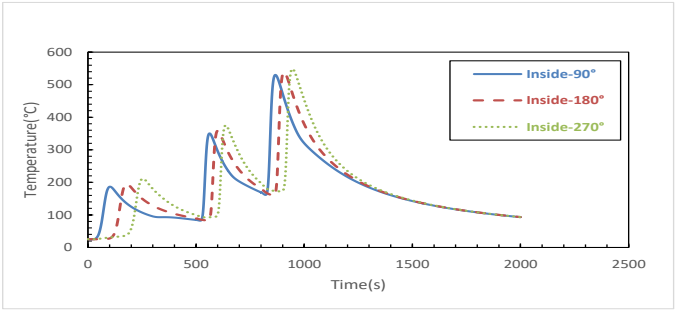

Figure 3.18: Thermal cycles at three locations on the inside surface at 14mm from the weld center for pipe 2.

In the outside surface:

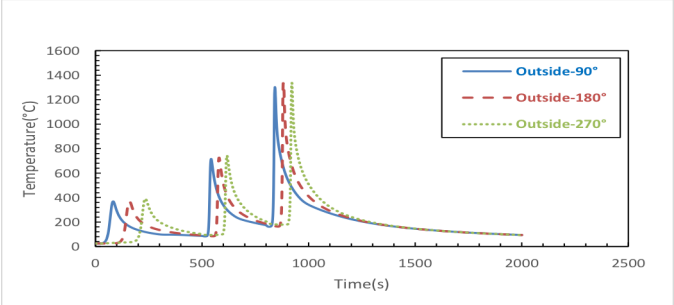

Figure 3.19: Thermal cycles at three locations on the outside surface at 3.5mm from the weld center for pipe 2.

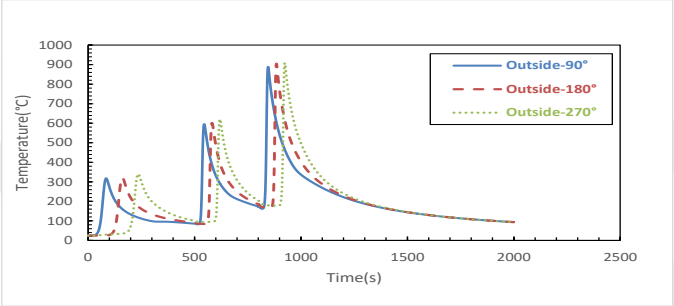

Figure 3.20: Thermal cycles at three locations on the outside surface at 6mm from the weld center for pipe 2.

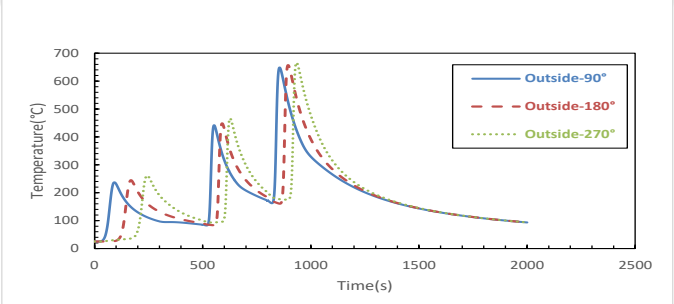

Figure 3.21: Thermal cycles at three locations on the outside surface at 10mm from the weld center for pipe 2.

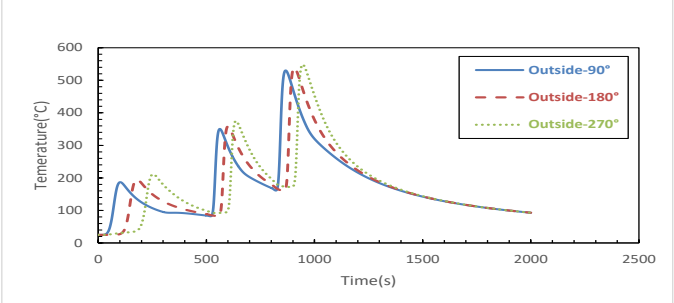

Figure 3.22: Thermal cycles at three locations on the outside surface at 14mm from the weld center for pipe 2.

3.6.1.3 Pipe number 3: Temperature Cycles for outer and inner surfaces

In the inside surface:

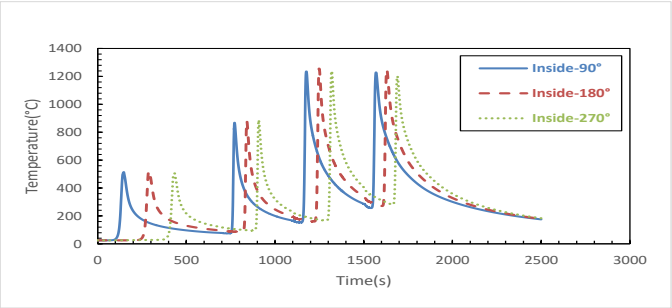

Figure 3.23: Thermal cycles at three locations on the inside surface at 4.5mm from the weld center for pipe 3.

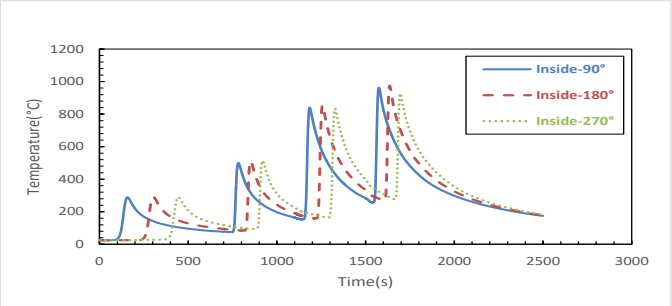

Figure 3.24: Thermal cycles at three locations on the inside surface at 10mm from the weld center for pipe 3.

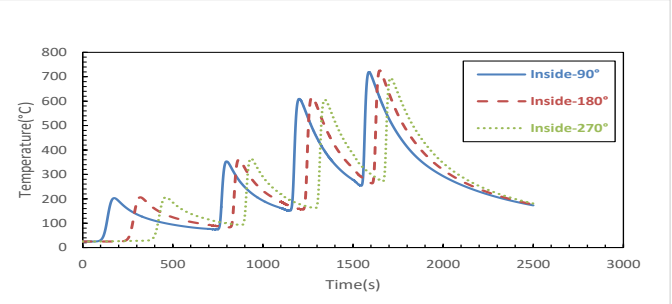

Figure 3.25: Thermal cycles at three locations on the inside surface at 15.5mm from the weld center for pipe 3.

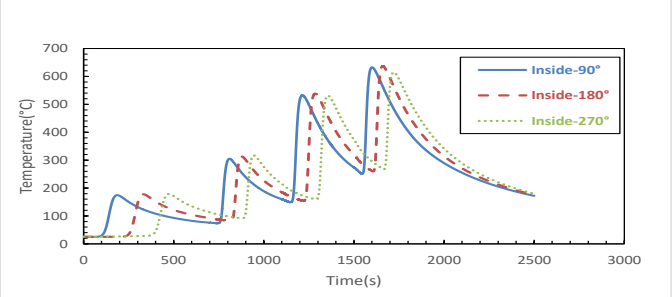

Figure 3.26: Thermal cycles at three locations on the inside surface at 19.5mm from the weld center for pipe 3.

In the outer surfaces:

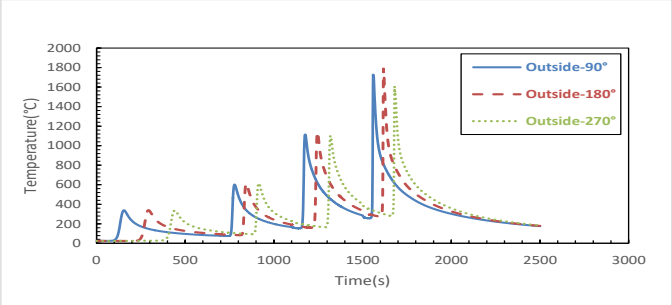

Figure 3.27: Thermal cycles at three locations on the outside surface at 5mm from the weld center for pipe 3.

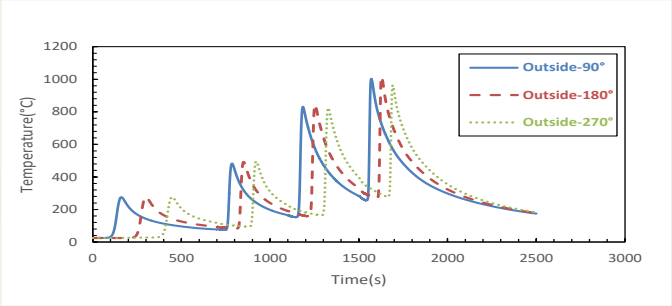

Figure 3.28: Thermal cycles at three locations on the outside surface at 10mm from the weld center for pipe 3.

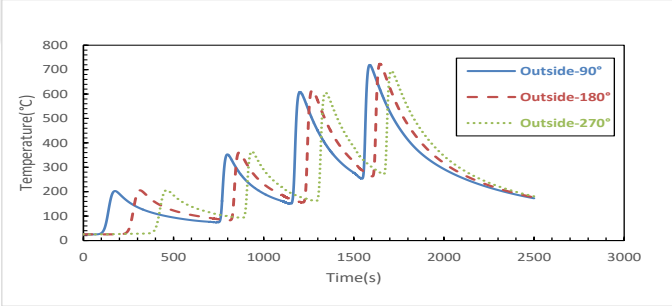

Figure 3.29: Thermal cycles at three locations on the outside surface at 15.5mm from the weld center for pipe 3.

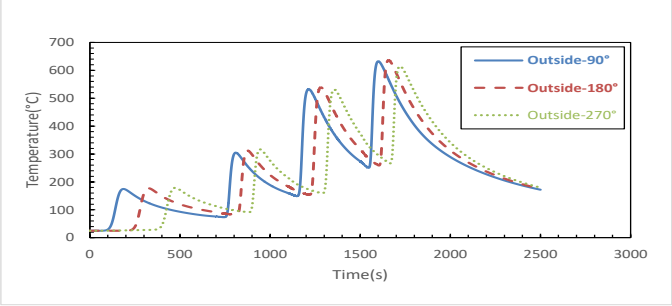

Figure 3.30: Thermal cycles at three locations on the outside surface at 19.5mm from the weld center for pipe 3.

3.6.1.4 Pipe number 4: Temperature Cycles at outer and inner surfaces

On the inside surface:

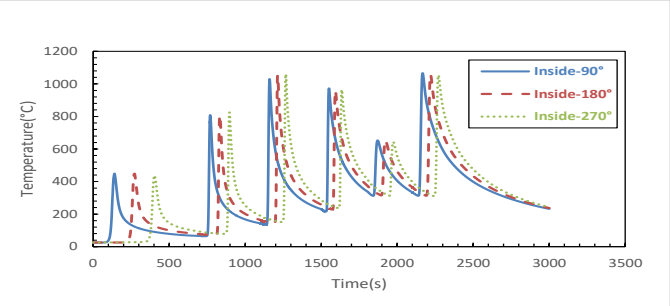

Figure 3.31: Thermal cycles at three locations on the inside surface at 5mm from the weld center for pipe 4.

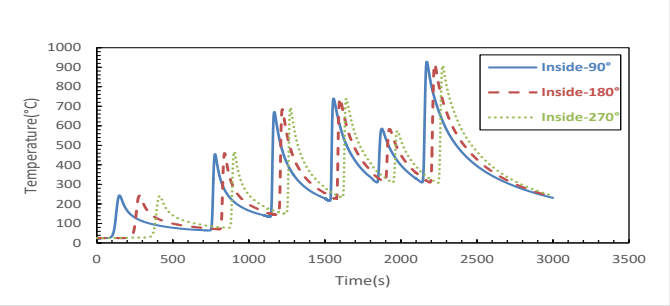

Figure 3.32: Thermal cycles at three locations on the inside surface at 10mm from the weld center for pipe 4.

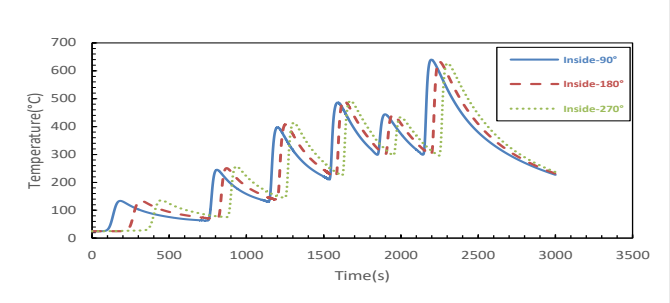

Figure 3.33: Thermal cycles at three locations on the inside surface at 20mm from the weld center for pipe 4.

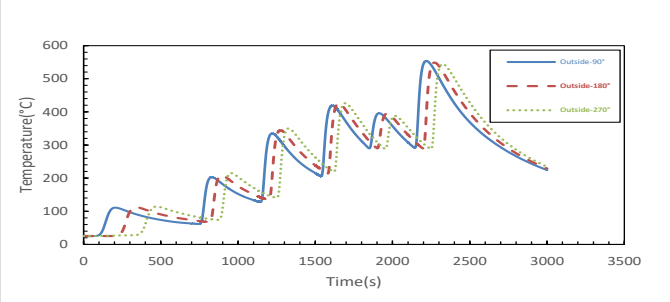

Figure 3.34: Thermal cycles at three locations on the outside surface at 25mm from the weld center for pipe 4.

On the outer surface:

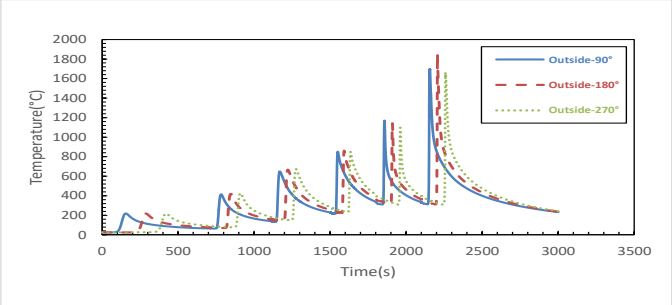

Figure 3.35: Thermal cycles at three locations on the outside surface at 7mm from the weld center for pipe 4.

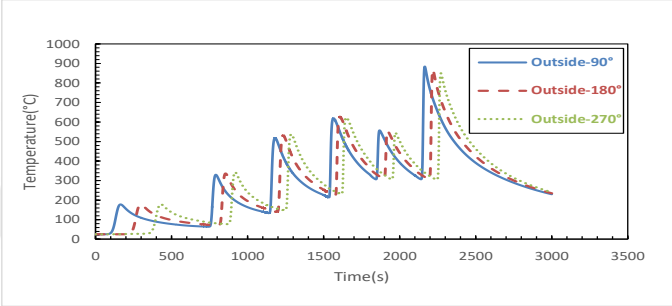

Figure 3.36: Thermal cycles at three locations on the outside surface at 13.5mm from the weld center for pipe 4.

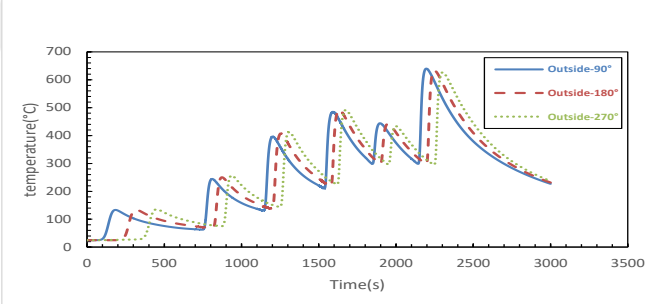

Figure 3.37: Thermal cycles at three locations on the outside surface at 20mm from the weld center for pipe 4.

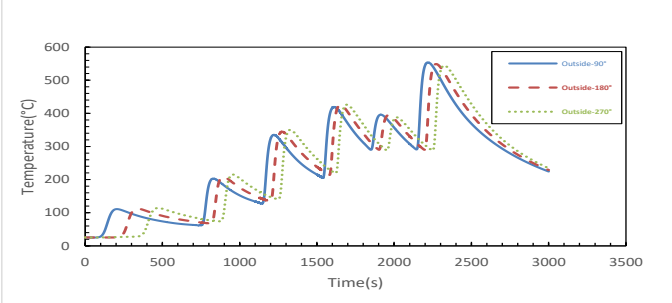

Figure 3.38: Thermal cycles at three locations on the outside surface at 25mm from the weld center for pipe 4.

3.6.2 Residual Stress Distribution

In this section, axial and hoop residual stress distributions on the inside and outside surfaces at different orientations in the modeled pipes are shown. According to these diagrams, in general, both the axial stress and the hoop stress are not significantly sensitive to the angle. It means that the stress distribution around the circumferential direction can be regarded as homogeneous distribution.

In the case of axial stress, on the inside surfaces, tensile residual stresses are generated near the weld zone and the HAZ, while compressive residual stresses are produced away from the weld zone and the HAZ. On the outside surface, compressive stresses can be seen at the weld zone, while relatively large tensile stresses are produced away from the weld zone. Comparing the axial residual stress distribution on the inside and outside surfaces, it is clear that the axial residual stress distribution on the inside surface is contrary to that on the outside surface. This phenomenon can be explained from the bending deformation produced by shrinkage in a radial direction at the weld zone.

For hoop stresses, at the weld zone and its vicinity, large tensile residual stresses are produced on both the inside surface and the outside surface. The large hoop residual stresses resulted from the relatively large restraint in the hoop direction.

When the pipe is butt-welded, the weld portion is shrunk both in the axial and circumferential directions. However, since both ends of the pipe are not restrained, the axial expansion and shrinkage do not cause an axial residual stress. On the other hand, most of the shrinkage of the pipe at the weld portion occurs when the deposited metal is solidified. This shrinkage introduces a tensile residual hoop stress homogeneously throughout the pipe wall thickness in the weld metal, balanced by compressive residual hoop stress away from the weld metal. For multipass welding, Since the formerly welded inner side layer is previously solidified, it becomes a constraint against the later welded outer side layer. Thus, the residual stress in the inner side is compressive, while the residual stress in the outer side is tensile both in the axial and circumferential directions. Since the circumferential shrinkage squeezes the inside of the pipe in the radial direction, the pipe at the weld metal is bent in the axial- radial plane. This bending deformation causes tensile residual stress at the inner surface and compressive resid- ual stress at the outer surface near the weld metal.

3.6.2.1 Pipe Number 1: axial and hoop residual stress distribution

Axial stresses distribution:

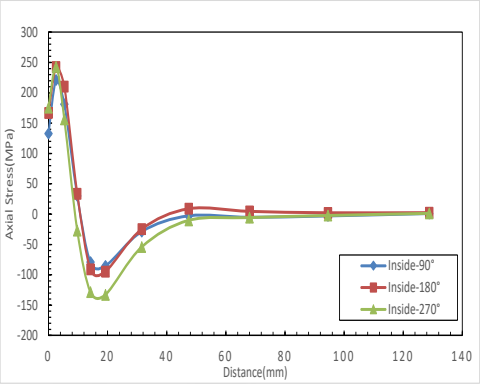

Figure 3.39: Axial stress distribution for various orientations from weld center on the inside surface for pipe 1.

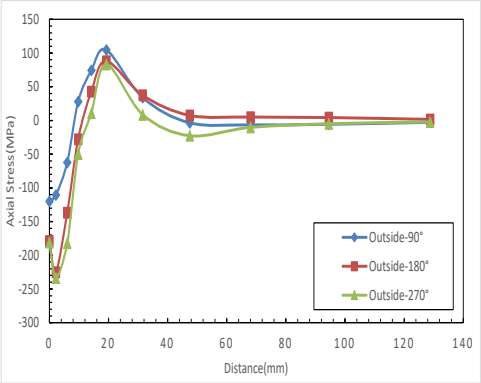

Figure 3.40: Axial stress distribution for various orientations from weld center on the outside surface for pipe 1.

Hoop stress distribution:

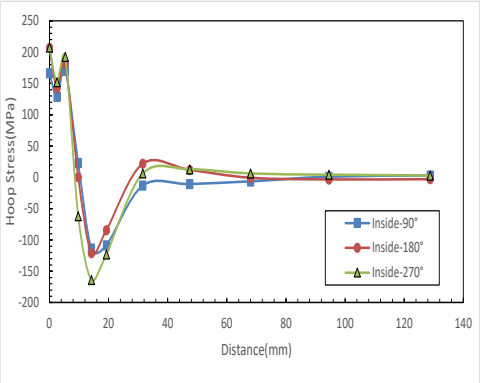

Figure 3.41: Hoop stress distribution for various orientations from weld center on the inside surface for pipe 1.

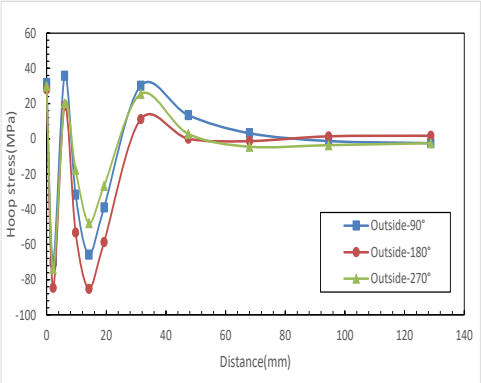

Figure 3.42: hoop stress distribution for various orientations from weld center on the outside surface for pipe 1.

3.6.2.2 Pipe Number 2: axial and hoop stress distribution

Axial stresses distribution:

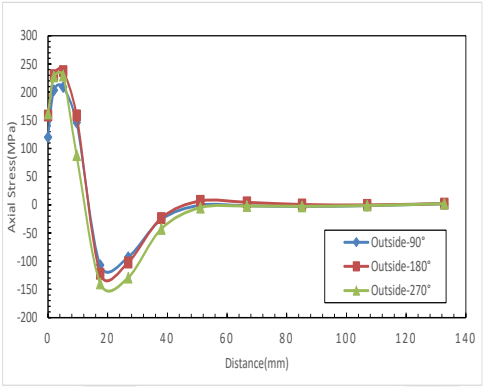

Figure 3.43: Axial stress distribution for various orientations from weld center on the inside surface for pipe 2.

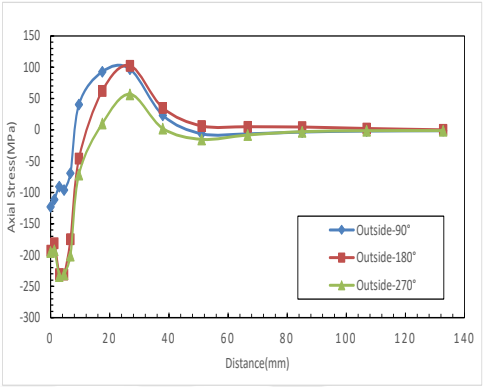

Figure 3.44: Axial stress distribution for various orientations from weld center on the outside surface for pipe 2.

Hoop stress distribution:

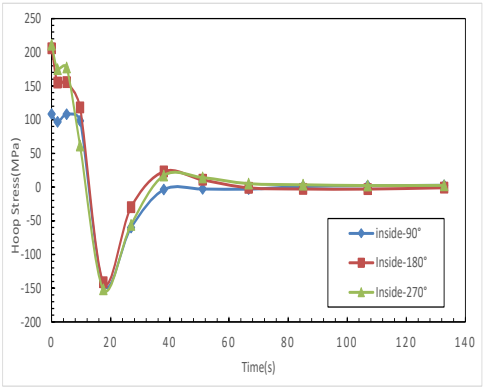

Figure 3.45: Hoop stress distribution for various orientations from weld center on the inside surface for pipe 2.

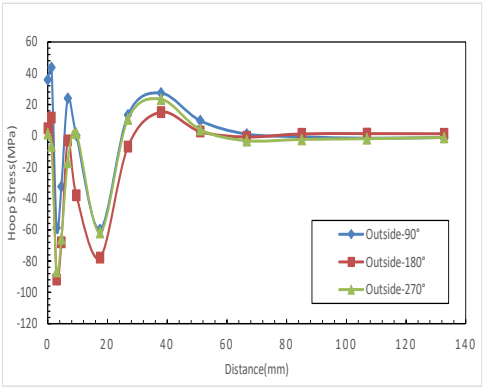

Figure 3.46: hoop stress distribution for various orientations from weld center on the outside surface for pipe 2.

3.6.2.3 Pipe Number 3: Axial and Hoop stress distribution

Axial stresses distribution:

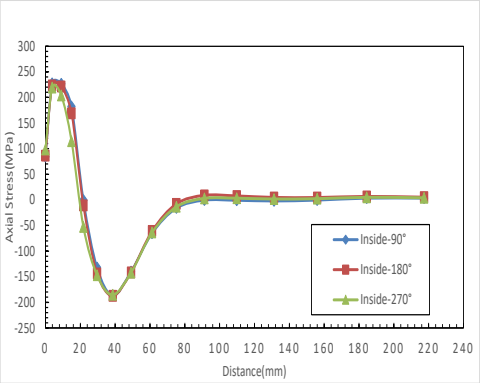

Figure 3.47: Axial stress distribution for various orientations from weld center on the inside surface for pipe 3.

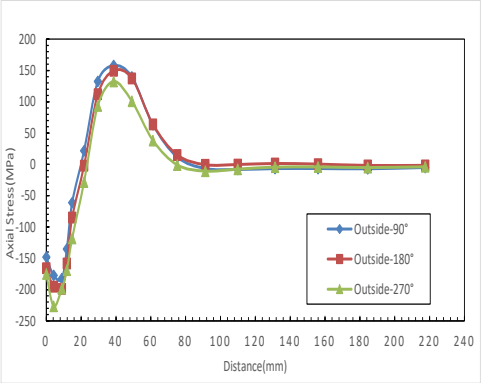

Figure 3.48: Axial stress distribution for various orientations from weld center on the outside surface for pipe 3.

Hoop stress distribution:

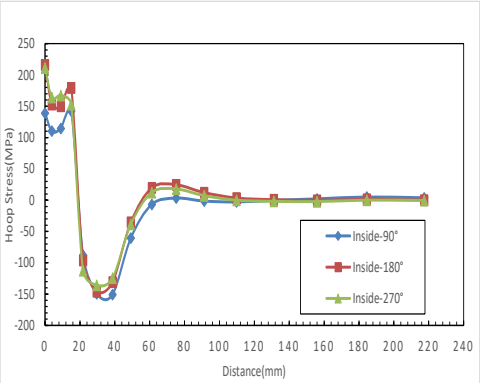

Figure 3.49: Hoop stress distribution for various orientations from weld center on the inside surface for pipe 3.

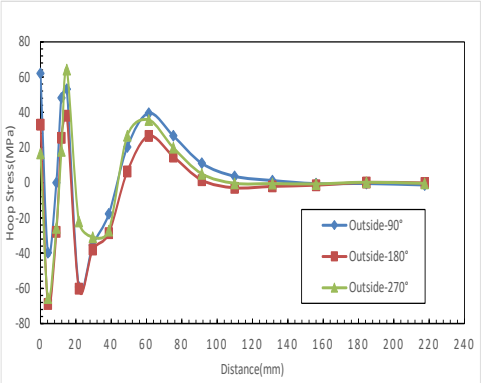

Figure 3.50: hoop stress distribution for various orientations from weld center on the outside surface for pipe 3.

3.6.2.4 Pipe Number 4: Axial and Hoop Stress distribution

Axial stresses distribution:

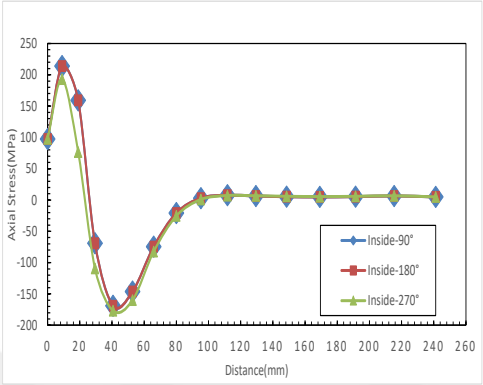

Figure 3.51: Axial stress distribution for various orientations from weld center on the inside surface for pipe 4.

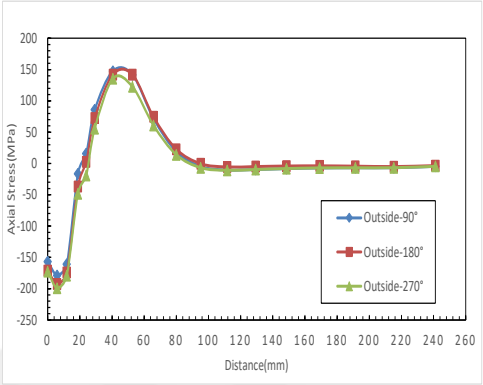

Figure 3.52: Axial stress distribution for various orientations from weld center on the outside surface for pipe 4.

Hoop stress distribution:

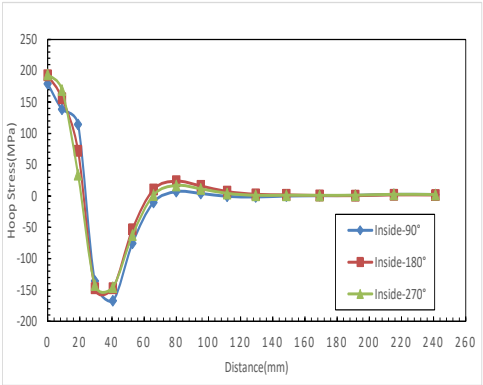

Figure 3.53: Hoop stress distribution for various orientations from weld center on the inside surface for pipe 4.

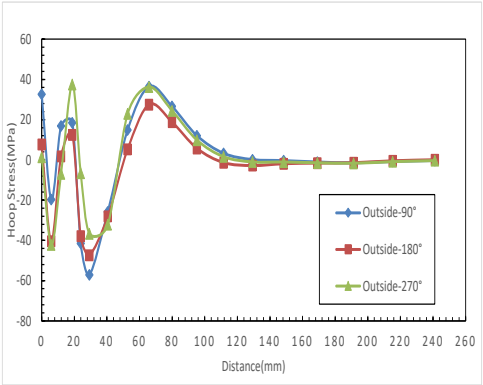

Figure 3.54: hoop stress distribution for various orientations from weld center on the outside surface for pipe 4.

3.6.3 HAZ ranges

As it is mentioned in past section, HAZ or heat affected zone is a part of base metal which are not subjected to that much of heat to melt but, as a result of experienced intensive temperature cycles, changes occur in its mechanical properties and microstructure.

By studying temperature fields obtained from thermal analyzes, HAZ length magnitude is figured out to apply these data in experimental investigation (table 3.4). It can be seen clearly, increasing in the thickness and consequently increasing in the number of passes results in higher heat inputs and it can shift up the magnetitue of HAZ length.

Table 3.4: HAZ lengths for Pipes welding.

PIPES	HAZ Width(mm)	HAZ length(mm)
Pipe 1	7	10
Pipe 2	8	12
Pipe 3	10	18
Pipe 4	14	22

4. EXPERIMENTAL WORKS

4.1 Material and methods

4.1.1 Welding proccess and material

Considering the obtained HAZ sizes from FEA, the experimental samples were prepared. For each pipe size, a pipe with length equals to twice the length of the estimated HAZ length was produced. In the next step, these small pipes were welded to two other pipes from both sides of it (figure 4.1). Since the welds are too close, the heat affected zones overlap in the middle pipe. The mechanical tests were done to analyze the overlapping section and compare this region with not overlapping HAZ's on the other side of pipes.

Figure 4.1 prepared welding models

As it told before, the welding type applied in this investigation is Tugesten Inert Gas (TIG) welding. All the weldings were carried out according to the situation mentioned

in the FE analizes. The groove angle for all the samples is 30°. The welding speed, voltage, current and interpass temperatures were organized according to table 3.3.

Finally using 308L welding rods the pipe in the middle was jointed to two pipes from both side of it (figure 4.2). The shielding gas was argon with the flow rate of 12-15 lit/min.

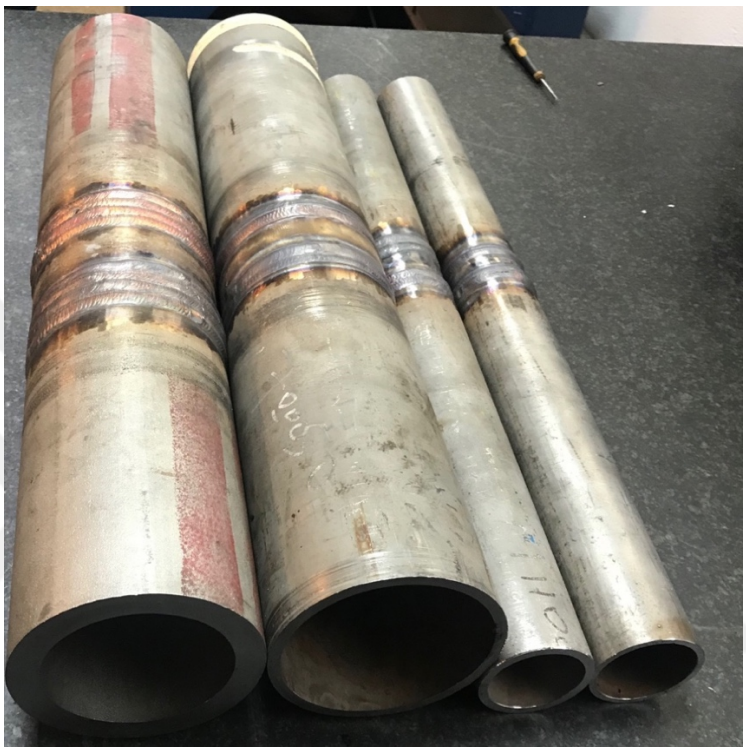

Figure 4.2: Welded Pipes.

4.1.2 Hardness Test

Hardness is defined as the resistance to indentation, and it is determined by measuring the permanent depth of the indentation. The hardness test is typically performed by measuring the depth of indenter penetration (Rockwell, Instrumented Indentation Testing, Ball Indentation Hardness) or by measuring the size of an impression left by an indenter (Vickers, Knoop and Brinell.) [26]. In this study, PROCEQ Equotip Bambino 2 Portable Hardness tester was used to evaluate hardness in different zones of welding (Figure 4-3). The working principle of this device is to derive the hardness in the means of the energy loss in the impact body after impacting on the metal sample [27]. This mechanism is called Leeb rebound hardness test. Impact energy exposed to the samples is 11.5Nmm.

The hardness value for various sections in this welding were measured. For each region, 3 different points hardnesses were measured and their average was declared as the hardness of that region. before the measurements, regions supposed to be examined were grinded coarsely. Information about selected sections are given in the results part.

Figure 4.3: PROCEQ Equotip Bambino 2 Portable Hardness tester collibration.

4.1.3 Tensile Testing

Tensile test in metals is a destructive test that studies materials behavior under controlled tension loading and significant mechanical information such as Yield Stress, ultimate tensile stress, elongation due to tentaion can be obtained through this analyzing process.

For tensile strength test, the tensile test samples were cut from the transverse section on the pipes including both consecutive weld zones. subsequently, the samples were machined according to TS EN ISO 4136 guidelines. The prepared samples are shown in figure 4-4. The Tensile Tests were done in the room temperature using a ASLA Universal Tensile Test Machine. (figure 4-6)

Figure 4.4: Tensile test samples.

Figure 4.5: ASLA Universal Tensile Test Machine.

4.1.4 Charpy Impact Testing

Charpy impact test (also known as Charpy V-notch test) is a destructive test that reveals the amount of energy absorbed during fracture by a material subjected to impact loading. This absorbed energy is a measure of the material's notch toughness.

The samples were cutted from the HAZ's overlapping section in the middle pipes (section 3) and in the other side HAZ with the same distance (section 5) from the weld center (figure 4.6). In the next step the cutted samples are machined according to TS EN ISO 148-1 standard guidelines (figure 4-6). The final samples are shown in the figure 4-7. In the last step, for studying the brittle behavior of material, all the samples were kept in liquid nitrogen to reach the -196°C temperature. For each region, three impac test samples were provided. ASLA 450J Impact test machine was used in this investigation(figure 4-9).

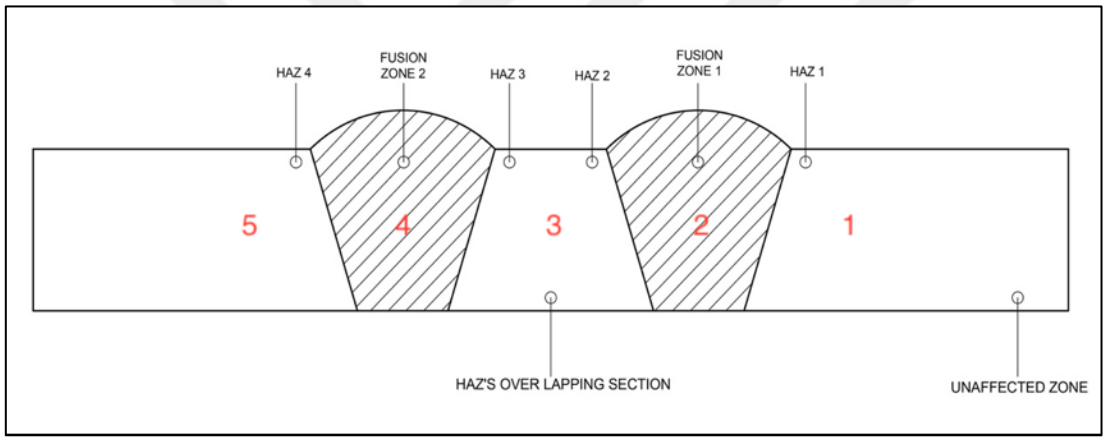

Figure 4.6: Different regions in teh final step

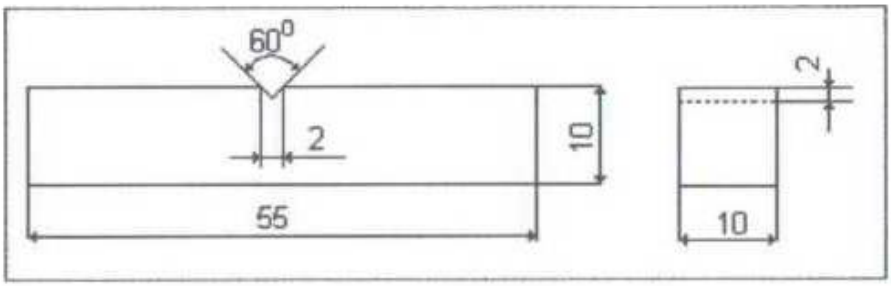

Figure 4.7: Impact Test samples geometry

Figure 4.8: Prepared Charpy Impact Test samples

Figure 4.9: ASLA 450J Impact Test Machine.

4.2 RESULTS AND DISCUSSION

4.2.1 Hardenss test results

Figure 5-1 demonstartes the different zone in which the hardness was measured. Average of three pints in each zone was reported as the hardness of according part.

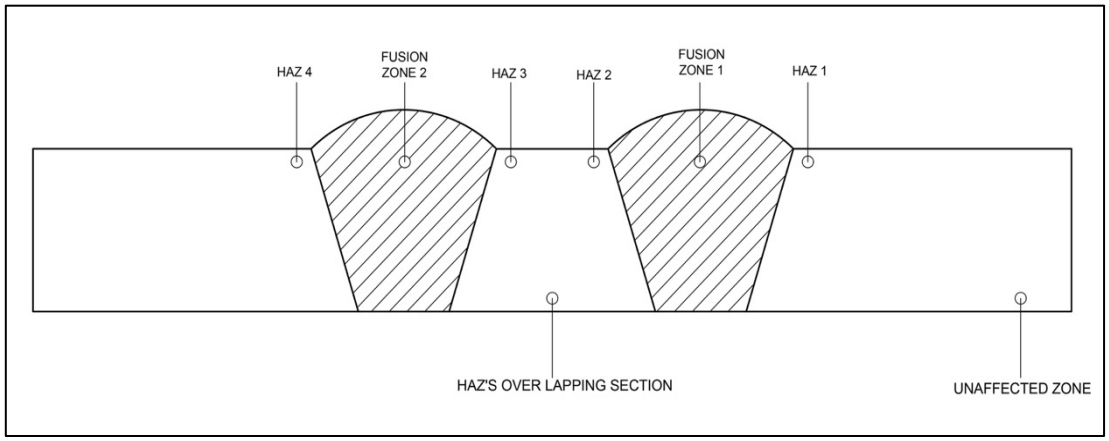

Figure 4.10: Hardness measured zones.

Brinel Hardness values for the specified sections are given in figure 5-1. According to obtained values, hardness demonstrates ascending manner by getting far away the fuszion zone which can be attributed to generated high residual stresses due to intensive heating in the HAZ zone [28]. As it can be anticipated, the minimum hardness belongs to the base metal zones in all samples. It is clear that for all the pipes, the maximum hardness is achieved in the overlapping section.

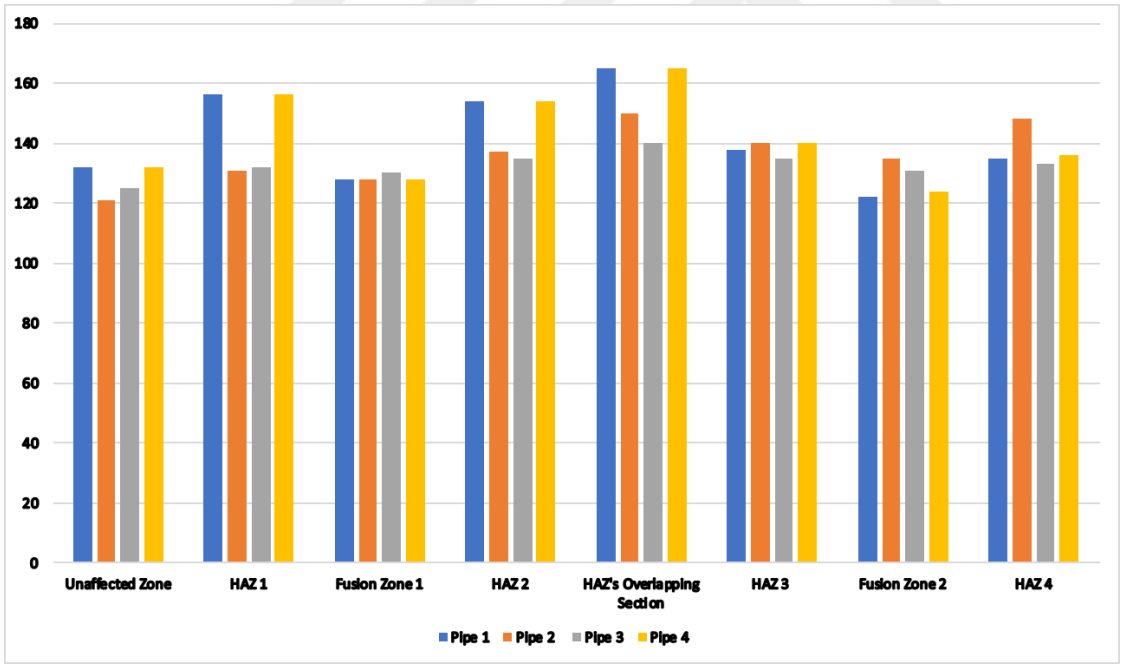

Figure 4.11: Measured Hardness For different zone

4.2.2 Tensile test results

The tensile samples were loaded until fracture to determine and evaluate the joint strength and performance at room temperature. Except sample related to pipe 1, all samples fractured in the HAZ'S overlapping region. It can be explained by overlapping generated tensile residual stresses, due to the high temperature gradient, in the middle

section. The tensile residual stresses of welding make the tensile elongation shorter [29]. For the pipe1, the centeres of pipes after welding were out of line in the second weld, it can be a reason to explain the fracture location.

Table 4.1: Tensile Test Results

Samples	Yield Strength (MPa)	Ultimate Tensile Strength(MPa)	Elongation	Fracture Location
PIPE 1	292.2	547.1	%24.2	HAZ 4
PIPE 2	366.2	582.6	%58.6	HAZ's Overlapping section
PIPE 3	342.9	612.6	%49.6	HAZ's Overlapping section
PIPE 4	413.2	606.2	%28.3	HAZ's Overlapping section

Figure 4.12: Fracture Locations

4.2.3 Charpy Impact Test resuts

The impacts toughness measurements for HAZ (region 5) and HAZ's overlapping section are shown in table 4.2. A drecease can be easily seen in the region 3 in all the samples.

Table 4.2: Impact toughness measures.

PIPES	PIPE 1		PIPE 2		PIPE 3		PIPE 4	
Measured Regions	Region 3	Region 5	Region 3	Region 5	Region 3	Region 5	Region 3	Region 5
Impact toughness In -196°C	30.04	34.27	35.50	37.97	38.87	40.06	184.32	199.51
	28.97	31.04	35.59	39.98	36.75	36.75	207.15	215.32
	32.23	31.13	34.46	37.13	34.41	38.25	191.85	208.74
Mean Impact Toughness	30.41	32.14	35.18	38.36	36.67	38.35	194.44	207.85

As it is told before, Existance of Chromium plays a significant role in increasing the resistance of stainless steel against corrosion, but in high temperatures in HAZ, because of Chromium precipitation as Chromium Carbid in grain boundries results in high hardness values in HAZ and decreases in mechanical properties of stainless steels due to brittle behavour of this phase [14]. This precipitation is done in 900-1150°C. by approaching to base metal, due to decreasing in welding temperature, toughness and mechanical properties are recovered usually [30]. But in the close welds due to existence of high tensile residual stresses instead of rising, the brittle toughness of HAZ is reduced.

5. CONCLUSIONS

In this study, the effects of adjacency of two butt welds in TIG welding of austenitic stainless-steel pipes were investigated. Four pipes with different outer diameters and wall thicknesses were subjected to this investigation. For the beginning, a finite element model was produced fore the multipass TIG welding of each pipe and the temperature distributions and residual stress (both axial and hoop stresses) distributions were obtained through simulations. In the experimental work, considering the length of HAZ measured from FEA, a pipe with a small thickness was welded to two pipes from both sides of it. And finally, hardness values, tensile properties and impact toughnesses of above-mentioned pipes were studied. Since expriencing intensive temperature cycles genereated from both consecutive multipass TIG weldments, the overlapping of HAZ's affected the mechanical properties (hardness, strength and ductility) of the small pipes located in the middle of the samples.

The outcome of this research is:

- A 3D Finite element model was developed to simulate the multipass TIG welding of 304L (austenitic stainless steel) pipes through ABAQUS software. The heat put source was modeled as in a double ellipsoidal distribution proposed by Goldak et al [25].
- Employing the simulated finite element modeling, the temperature distribution and residual stress distribution on the inner and outer surfaces can be plotted.
- Based on FEA, it is obvious that the temperature distribution is steady in different orientations (90°,180°and 270°)when the welding torch moves around the stainless steel pipe.
- Consedring results obtained from FEA, the residual stress on both outside and inside surfaces has a homogenous distribution in different orientations (90°,180°and 270°).

- In the outer surface, the residual axial stress is compressive in fusion zone and the HAZ zone the residual axial stress is tensile. The reverse condtion is generated in inside surface where the residual axial stress is tensile in fuzion zone and compressive in HAZ.
- For hoop stresses, at the weld zone and its vicinity, large tensile residual stresses are produced on both the inside surface and the outside surface.
- The length of haz increases by increasing in the thickness and number of welding passes.
- The maximum value of hardness is achieved in HAZ's overlapping section in the middle pipes. It can be as an effect of intensified compressive hoop stress generated in the middle zone (overlapping generated stresses from consecutive weldings) and precitipation of chorioum carbid.
- All the samples except sample related to pipe 1, fractured from the overlapping section. It can attribute to the intensified axial residual tensile stresses which reduced the elongation and leads to fracture. a defect in aligment of pipes is the reason of fracture in fusion zone of pipe 1.
- Comparsion between brittle toughness of region 3(HAZ unaffected from other welding) and region 5 (HAZ's overlapping section) shows a decrease in overlapping section. Which is in agreement with tensile tests.
- Two close welds can affect each other mechanical properties since the minimum distance between two consecutive welds should be more than sum of length of their HAZ's.

REFERENCES

[1] **Url-1** <http://www.fluidmotorunion.com/differential-strokes> , date retrived 1-4-2018.

[2] **Kou,S .**,(2003)." WELDING METALLURGY", New Jersey: John Wiley & Sons Inc.

[3] **m. Vladimir, L. jinsun, k. IKEUCHI, T. KURODA, Y. KIKUCHI and F. MATSUDA**,.(1996). "New Aspects of Sensitization Behavior in Recent 316 Type Austenitic Stainless Steels," Osaka University knowlege archive, Osaka.

[4] **J. Winczek, G. Rygał and T. Skrzypcza,**(2015), "THE MODEL OF TEMPORARY TEMPERATURE FIELD DURING MULTI-PASS ARC WELD SURFACING. PART I: ANALYTICAL DESCRIPTION," *Journal of Applied Mathematics and Computational Mechanics,* pp. 123-130.

[5] **O. Obeid , G. Alfano, H. Bahai and H. Jo**,(2017), "A parametric study of thermal and residual stress fields in lined pipe welding," *Thermal Science and Engineering Progress*.

[6] **H. Cerjak,**(2008) "The Role of Welding in the Power Generation Industry," *Proceedings of the International Conference Safety and Reliability of Welded Components,* pp. 17-27.

[7] **L. LiYing, H. Tao and L. ChaoWen,**(2011), "Embrittlement and toughening in CGHAZ of ASTM4130 steel," *SCIENCE CHINA Physics, Mechanics & Astronomy,* pp. 1447-1454.

[8] **L.-y. Li, Y. Wang and C.-w. Li,**(2010), "Microstructure and embrittlement of the fine-grained heat-affected zone of ASTM4130 steel," *International Journal of Minerals, Metallurgy and Materials,* pp. 419-424, 2010.

[9] **J. Nicholas and . D. Abson,**(2008) "The prediction of maximum HAZ hardness in various regions of multiple pass welds," in *Computer Technology in Welding and Engineering*, Cranfield.

[10] **C. Lee, R. Chandel and S. Seow**,(2005), "Effect of Welding Parameters on the Size of Heat Affected Zone of Submerged Arc Welding," *Materials and manufaturing Procesesses,* vol. 15, no. 5, pp. 649-666.

[11] **E. Cureil-Reyna, A. Herrera, V. Castano and M. Rodriguez,**(2005), "Influence of Cooling Rate on the Structure of Heat Affected Zone After Welding a High Manganese Ste," *Materials and Manufacturing Processes,* vol. 20, no. 5, pp. 813-822.

[12] F. Shehata,(1994),"Effect of plate thickness on mechanical properties of steel arc welded joints," Zagazig University,, Zagazig.

[13] J. Rajakumar, M. Sheik Ibrahim Bathusa, N. Pothivel Rajan, K. Sulaiman, A. Simon Christopher and K. C. Ganesh,(2017), "Numerical Investigation of Heat Transfer Behaviour During TIG Welding of Stainless Steel Pipes for Various Welding Heat Input Conditions," *American Journal of Mechanical and Industrial Engineering,* pp. 117-123.

[14] R. S. C. &. H. P. S. C. S. Lee,(2000), "Effect of Welding Parameters on the Size of Heat Affected Zone of Submerged Arc Welding," *Materials and Manufacturing Processes,* vol. 15:5, pp. 649-666.

[15] T. Singh, A. Shahi and M. kaur,(2013), "EXPERIMENTAL STUDIES ON THE EFFECT OF MULTIPASS WELDING ON THE MECHANICAL PROPERTIES OF AISI 304 STAINLESS STEEL SMAW JOINTS," *International Journal of Scientific & Engineering Research,,* vol. 4, no. 12, pp. 951-961.

[16] J. Davis,(1994), ASM Specialty Handbook: Stainless Steels, ASM International.

[17] C. F. Willis,(1990),"A STUDY OF CHROMIUM CARBIDE PRECIPITATION" AT INTERPHASE BOUNDARIES IN STAINLESS STEEL WELDS," University of California, Berkeley,California, Berkeley.

[18] J. Varghese , Suresh and S. Kumar,(2012), "Recent developments in modeling of heat transfer during TIG welding—a review," Springer-Verlag, london.

[19] Y. Ueda, K. Fukuda and Y. Kim, (1986),"New measuring method of axisymmetric three-dimensional residual stresses using inherent strains as parameters," *Journal of Engineering Materials and Technology,,* pp. 328-334.

[20] B. Brickstad and B. Josefson,(1998), "A parametric study of residual stresses in multi-pass butt-welded stainless steel pipes.”," *International Journal of Pressure Vessels and Piping,,* pp. 11-25.

[21] M. Mochizuki, M. Hayashi and T. Hattori,(2000), "Numerical analysis of welding residual stress and its verification using neutron diffraction measurement," *Journal of Engineering Materials and Technology,,* pp. 98-103.

[22] K.-H. Chang, C.-H. Lee and . K.-T. Par,(2010), "Analysis of Residual Stress in Stainless Steel Pipe Weld Subject to Mechanical Axial Tension Loading," *International Journal of Steel Structures,* pp. 411-418.

[23] D. Deng and H. Murakawa,(2008), "Numerical simulation of temperature field and residual stress in multi-pass welds in stainless steel pipe and comparison with experimental measurements," Osaka University, Osaka.

[24] P. Duranton, J. Devauxa, V. Robin and P. Gilles,(2004), "3D modelling of multipass welding of a 316L stainless steel pipe," *Journal of Materials Processing Technology,* pp. 457-463.

[25] **X. Lu and T. Hassan,**(2001), "Residual Stresses in Butt and Socket Welded Joints," Center for Nuclear Power Plant Structures, North Carolina State University, Raleigh, NC.

[26] **V. Prasad , J. Varghese and Suresh,**(2016), "3D simulation of residual stress developed during TIG welding of stainless steel pipes," in *International Conference on Emerging Trends in Engineering, Science and Technology*, Kerala.

[27] **J. Argyris, J. Szimmat and K. Willam,**(1982), "Computational aspects of welding stress analysis," *Computer methods in applied mechanics and engineering,* pp. 635-665.

[28] **J. GOLDAK, A. CHAKRAVARTI and M. BIBBY,**(1983), "A new finite element model for welding heat sources," *Metallurgical and Materials Transactions B,* pp. 299-305.

[29] **R. L. Chinn,**(2009),"Hardness, bearings, and the Rockwells," *Advanced Materials & Processes,* vol. 167, no. 10, pp. 29-31.

[30] **Url-2** <https://en.wikipedia.org/wiki/Leeb_rebound_hardness_test#cite_ref-3>. date retrived 10-2-2018.

[31] **K. Tosha,**(2002), "Influence of Residual Stresses on the Hardness Number in the Affected Layer Produced by Shot Peening," in *2nd Asia-Pacific Forum on Precision Surface Finishing and Deburring Technology*, Seoul, Korea.

[32] **B. C. G. a. S. Y. Yang,**(2008), "Finite Element Analysis of the Effect of Residual Stress on Mechanical Behavior of Welded Plates," in *Trans Tech Publications*, Switzerland.

[33] **Hyun-Seop Shin, Ki-Tae Park,**(2015)"Low Temperature Impact Toughness of Structural Steel Welds with Different Welding Processes," *KSCE Journal of Civil Engineering,* pp. 1-7.

APPENDICES

APPANDIX A.1: Subroutine codes for modeling heat input and heat loss in PIPE 1.
APPANDIX A.2: Subroutine codes for modeling heat input and heat loss in PIPE 2.
APPANDIX A.3: Subroutine codes for modeling heat input and heat loss in PIPE 3.
APPANDIX A.4: Subroutine codes for modeling heat input and heat loss in PIPE 4.
APPANDIX A.5: Hardness measurments in all pipes after welding.
APPANDIX A.6: Stress-Strain curves obtained from tensile tests.

APPANDIX A.1:

Subroutine codes for modeling heat input and heat loss in PIPE 1

```
      SUBROUTINE DFLUX(FLUX,SOL,KSTEP,KINC,TIME,NOEL,NPT,COORDS,
     1 JLTYP,TEMP,PRESS,SNAME)
C
      INCLUDE 'ABA_PARAM.INC'
C
      DIMENSION FLUX(2),TIME(2),COORDS(3)
      CHARACTER*80 SNAME
      A=0.01
      B=0.005
      CR=0.008
      CF=0.006
      FR=1.15
      FF=0.85
      EF=0.7
      do i=1,time(2)
!------------------- ----------------------------    Pass 1
      if(time(2)<319.8)then
      tt=op*i*pc
      deo=0.05448
      v=0.000545
      pe=deo*3.14
      po=pe/v
      pc=360/po
      Q=991
      op=3.14/180
      yp=(coords(2)*cos(tt)+coords(3)*sin(tt))-deo/2
      zp=coords(2)*sin(tt)-coords(3)*cos(tt)
      if(jltyp.eq.1)then
      if(zp<0)then
      WA=sqrt(3.0)
      WB=(3.14)**(3/2)
      wr=6*WA*FF*Q/(A*B*CF*WB)
      wt=EXP(-3*(x**2/(A**2)))
      wy=EXP(-3*(yp**2/(B**2)))
      WU=EXP(-3*(zp**2/(CF**2)))
      flux(1)=WR*WT*WY*WU
      end if
      if(zp>0)then
      WA=3**(1/2)
      WB=(3.14)**(3/2)
      wr=6*WA*Fr*Q/(A*B*Cr*WB)
      wt=EXP(-3*(x**2/(A**2)))
      wy=EXP(-3*(yp**2/(B**2)))
      WU=EXP(-3*(zp**2/(Cr**2)))
      flux(1)=WR*WT*WY*WU
      END IF
      END IF
      END IF
!-------------------------------------------------------  cooling 1
      if(319.8<time(2) .AND. 500>time(2))then
      pe=deo*3.14
      v=0.000545
      po=pe/v
      pc=360/po
      Q=0
      if(zp<0)then
      flux(1)=0
      end if
      if(zp>0)then
      flux(1)=0
      END IF
```

```
      END IF

! ------------------------------------------------------------------------ pass 2
      if(500<time(2) .AND. 657.87>time(2))then
      tt=op*(i-500)*pc
      deo=0.0603
      v=0.0012
      pe=deo*3.14
      po=pe/v
      pc=360/po
      Q=1092
      op=3.14/180
      yp=(coords(2)*cos(tt)+coords(3)*sin(tt))-deo/2
      zp=coords(2)*sin(tt)-coords(3)*cos(tt)
      if(jltyp.eq.1)then
      if(zp<0)then
      WA=sqrt(3.0)
      WB=(3.14)**(3/2)
      wr=6*WA*FF*Q/(A*B*CF*WB)
      wt=EXP(-3*(x**2/(A**2)))
      wy=EXP(-3*(yp**2/(B**2)))
      WU=EXP(-3*(zp**2/(CF**2)))
      flux(1)=WR*WT*WY*WU
      end if
      if(zp>0)then
      WA=3**(1/2)
      WB=(3.14)**(3/2)
      wr=6*WA*Fr*Q/(A*B*Cr*WB)
      wt=EXP(-3*(x**2/(A**2)))
      wy=EXP(-3*(yp**2/(B**2)))
      WU=EXP(-3*(zp**2/(Cr**2)))
      flux(1)=WR*WT*WY*WU
      END IF
      END IF
      END IF
!------------------------------------------------------------ cooling 2


      end do
      RETURN
      END

       SUBROUTINE FILM(H,SINK,TEMP,KSTEP,KINC,TIME,NOEL,NPT,
     1 COORDS,JLTYP,FIELD,NFIELD,SNAME,NODE,AREA)
C
      INCLUDE 'ABA_PARAM.INC'
C
      DIMENSION H(2),TIME(2),COORDS(3),FIELD(NFIELD)
      CHARACTER*80 SNAME
      do i=1,time(2)
      do j=50,temp
      if(temp<500)then
      sink=25
      h(1)=0.068*temp
      else
      h(1)=0.231*temp-81.5
      end if
      end do
      end do
      RETURN
      END
```

APPANDIX A.2:

Subroutine codes for modeling heat input and heat loss in PIPE 2.

```
      SUBROUTINE DFLUX(FLUX,SOL,KSTEP,KINC,TIME,NOEL,NPT,COORDS,
     1 JLTYP,TEMP,PRESS,SNAME)
C
      INCLUDE 'ABA_PARAM.INC'
C
      DIMENSION FLUX(2),TIME(2),COORDS(3)
      CHARACTER*80 SNAME
      A=0.01
      B=0.005
      CR=0.008
      CF=0.006
      FR=1.15
      FF=0.85
      EF=0.7
      do i=1,time(2)
!------------------- ----------------------------          Pass 1
      if(time(2)<302)then
      tt=op*i*pc
      deo=0.05222
      v=0.000545
      pe=deo*3.14
      po=pe/v
      pc=360/po
      Q=990
      op=3.14/180
      yp=(coords(2)*cos(tt)+coords(3)*sin(tt))-deo/2
      zp=coords(2)*sin(tt)-coords(3)*cos(tt)
      if(jltyp.eq.1)then
      if(zp<0)then
      WA=sqrt(3.0)
      WB=(3.14)**(3/2)
      wr=6*WA*FF*Q/(A*B*CF*WB)
      wt=EXP(-3*(x**2/(A**2)))
      wy=EXP(-3*(yp**2/(B**2)))
      WU=EXP(-3*(zp**2/(CF**2)))
      flux(1)=WR*WT*WY*WU
      end if
      if(zp>0)then
      WA=3**(1/2)
      WB=(3.14)**(3/2)
      wr=6*WA*Fr*Q/(A*B*Cr*WB)
      wt=EXP(-3*(x**2/(A**2)))
      wy=EXP(-3*(yp**2/(B**2)))
      WU=EXP(-3*(zp**2/(Cr**2)))
      flux(1)=WR*WT*WY*WU
      END IF
      END IF
      END IF
!-----------------------------------------------------          cooling 1
      if(302<time(2) .AND. 500>time(2))then
      pe=deo*3.14
      v=0.000545
      po=pe/v
      pc=360/po
      Q=0
      if(zp<0)then
      flux(1)=0
      end if
      if(zp>0)then
      flux(1)=0
      END IF
```

```
    END IF

! ------------------------------------------------------------------------ pass 2
    if(500<time(2) .AND. 648>time(2))then
    tt=op*(i-500)*pc
    deo=0.05662
    v=0.0012
    pe=deo*3.14
    po=pe/v
    pc=360/po
    Q=1090
    op=3.14/180
    yp=(coords(2)*cos(tt)+coords(3)*sin(tt))-deo/2
    zp=coords(2)*sin(tt)-coords(3)*cos(tt)
    if(jltyp.eq.1)then
    if(zp<0)then
    WA=sqrt(3.0)
    WB=(3.14)**(3/2)
    wr=6*WA*FF*Q/(A*B*CF*WB)
    wt=EXP(-3*(x**2/(A**2)))
    wy=EXP(-3*(yp**2/(B**2)))
    WU=EXP(-3*(zp**2/(CF**2)))
    flux(1)=WR*WT*WY*WU
    end if
    if(zp>0)then
    WA=3**(1/2)
    WB=(3.14)**(3/2)
    wr=6*WA*Fr*Q/(A*B*Cr*WB)
    wt=EXP(-3*(x**2/(A**2)))
    wy=EXP(-3*(yp**2/(B**2)))
    WU=EXP(-3*(zp**2/(Cr**2)))
    flux(1)=WR*WT*WY*WU
    END IF
    END IF
    END IF
!------------------------------------------------------------  cooling 2
    if(648<time(2) .AND. 800>time(2))then
    pe=deo*3.14
    v=0.0012
    po=pe/v
    pc=360/po
    Q=0
    if(zp<0)then
    flux(1)=0
    end if
    if(zp>0)then
    flux(1)=0
    END IF
    END IF
! ------------------------------------------------------------------------ pass 3
    if(800<time(2))then
    tt=op*(i-800)*pc
    deo=0.0603
    v=0.0012
    pe=deo*3.14
    po=pe/v
    pc=360/po
    Q=1180
    op=3.14/180
    yp=(coords(2)*cos(tt)+coords(3)*sin(tt))-deo/2
    zp=coords(2)*sin(tt)-coords(3)*cos(tt)
    if(jltyp.eq.1)then
    if(zp<0)then
    WA=sqrt(3.0)
    WB=(3.14)**(3/2)
    wr=6*WA*FF*Q/(A*B*CF*WB)
    wt=EXP(-3*((x+0.002)**2/(A**2)))
```

```
      wy=EXP(-3*(yp**2/(B**2)))
      WU=EXP(-3*(zp**2/(CF**2)))
      flux(1)=WR*WT*WY*WU
      end ifx
      if(zp>0)then
      WA=3**(1/2)
      WB=(3.14)**(3/2)
      wr=6*WA*Fr*Q/(A*B*Cr*WB)
      wt=EXP(-3*(x**2/(A**2)))
      wy=EXP(-3*(yp**2/(B**2)))
      WU=EXP(-3*(zp**2/(Cr**2)))
      flux(1)=WR*WT*WY*WU
      END IF
      END IF
      END IF
!------------------------------------------------------  cooling 3

      end do
      RETURN
      END

       SUBROUTINE FILM(H,SINK,TEMP,KSTEP,KINC,TIME,NOEL,NPT,
     1 COORDS,JLTYP,FIELD,NFIELD,SNAME,NODE,AREA)
C
      INCLUDE 'ABA_PARAM.INC'
C
      DIMENSION H(2),TIME(2),COORDS(3),FIELD(NFIELD)
      CHARACTER*80 SNAME
      do i=1,time(2)
      do j=50,temp
      if(temp<500)then
      sink=25
      h(1)=0.068*temp
      else
      h(1)=0.231*temp-81.5
      end if
      end do
      end do
      RETURN
      END
```

APPANDIX A.3:

Subroutine codes for modeling heat input and heat loss in PIPE 3.

```
      SUBROUTINE DFLUX(FLUX,SOL,KSTEP,KINC,TIME,NOEL,NPT,COORDS,
     1 JLTYP,TEMP,PRESS,SNAME)
C
      INCLUDE 'ABA_PARAM.INC'
C
      DIMENSION FLUX(2),TIME(2),COORDS(3)
      CHARACTER*80 SNAME
      A=0.006
      B=0.005
      CR=0.015
      CF=0.005
      FR=1.15
      FF=0.85
      EF=0.73
      do i=1,time(2)
!------------------- ----------------------------  Pass 1
      if(time(2)<566.95)then
      tt=op*i*pc
      deo=0.09818
      v=0.000545
      pe=deo*3.14
      po=pe/v
      pc=360/po
      Q=991
      op=3.14/180
      yp=(coords(2)*cos(tt)+coords(3)*sin(tt))-deo/2
      zp=coords(2)*sin(tt)-coords(3)*cos(tt)
      if(jltyp.eq.1)then
      if(zp<0)then
      WA=sqrt(3.0)
      WB=(3.14)**(3/2)
      wr=6*WA*FF*Q/(A*B*CF*WB)
      wt=EXP(-3*(x**2/(A**2)))
      wy=EXP(-3*(yp**2/(B**2)))
      WU=EXP(-3*(zp**2/(CF**2)))
      flux(1)=WR*WT*WY*WU
      end if
      if(zp>0)then
      WA=3**(1/2)
      WB=(3.14)**(3/2)
      wr=6*WA*Fr*Q/(A*B*Cr*WB)
      wt=EXP(-3*(x**2/(A**2)))
      wy=EXP(-3*(yp**2/(B**2)))
      WU=EXP(-3*(zp**2/(Cr**2)))
      flux(1)=WR*WT*WY*WU
      END IF
      END IF
      END IF
!------------------------------------------------------------ cooling 1
      if(566.95<time(2) .AND. 700>time(2))then
      pe=deo*3.14
      v=0.000545
      po=pe/v
      pc=360/po
      Q=0
      if(zp<0)then
      flux(1)=0
      end if
      if(zp>0)then
      flux(1)=0
      END IF
```

```
    END IF

! ------------------------------------------------------------------- pass 2
    if(700<time(2) .AND. 970.12>time(2))then
    tt=op*(i-700)*pc
    deo=0.10318
    v=0.0012
    pe=deo*3.14
    po=pe/v
    pc=360/po
    Q=1092
    op=3.14/180
    yp=(coords(2)*cos(tt)+coords(3)*sin(tt))-deo/2
    zp=coords(2)*sin(tt)-coords(3)*cos(tt)
    if(jltyp.eq.1)then
    if(zp<0)then
    WA=sqrt(3.0)
    WB=(3.14)**(3/2)
    wr=6*WA*FF*Q/(A*B*CF*WB)
    wt=EXP(-3*(x**2/(A**2)))
    wy=EXP(-3*(yp**2/(B**2)))
    WU=EXP(-3*(zp**2/(CF**2)))
    flux(1)=WR*WT*WY*WU
    end if
    if(zp>0)then
    WA=3**(1/2)
    WB=(3.14)**(3/2)
    wr=6*WA*Fr*Q/(A*B*Cr*WB)
    wt=EXP(-3*(x**2/(A**2)))
    wy=EXP(-3*(yp**2/(B**2)))
    WU=EXP(-3*(zp**2/(Cr**2)))
    flux(1)=WR*WT*WY*WU
    END IF
    END IF
    END IF
!---------------------------------------------------------- cooling 2
    if(970.12<time(2) .AND. 1100>time(2))then
    pe=deo*3.14
    v=0.0012
    po=pe/v
    pc=360/po
    Q=0
    if(zp<0)then
    flux(1)=0
    end if
    if(zp>0)then
    flux(1)=0
    END IF
    END IF
! ------------------------------------------------------------------- pass 3
    if(1100<time(2) .AND. 1382.5>time(2))then
    tt=op*(i-1100)*pc
    deo=0.1079
    v=0.0012
    pe=deo*3.14
    po=pe/v
    pc=360/po
    Q=1180
    op=3.14/180
    yp=(coords(2)*cos(tt)+coords(3)*sin(tt))-deo/2
    zp=coords(2)*sin(tt)-coords(3)*cos(tt)
    if(jltyp.eq.1)then
    if(zp<0)then
    WA=sqrt(3.0)
    WB=(3.14)**(3/2)
    wr=6*WA*FF*Q/(A*B*CF*WB)
    wt=EXP(-3*(x**2/(A**2)))
```

```
      wy=EXP(-3*(yp**2/(B**2)))
      WU=EXP(-3*(zp**2/(CF**2)))
      flux(1)=WR*WT*WY*WU
      end if
      if(zp>0)then
      WA=3**(1/2)
      WB=(3.14)**(3/2)
      wr=6*WA*Fr*Q/(A*B*Cr*WB)
      wt=EXP(-3*(x**2/(A**2)))
      wy=EXP(-3*(yp**2/(B**2)))
      WU=EXP(-3*(zp**2/(Cr**2)))
      flux(1)=WR*WT*WY*WU
      END IF
      END IF
      END IF
!------------------------------------------------------------ cooling 3
      if(1382.5<time(2) .AND. 1500>time(2))then
      pe=deo*3.14
      v=0.0012
      po=pe/v
      pc=360/po
      Q=0
      if(zp<0)then
      flux(1)=0
      end if
      if(zp>0)then
      flux(1)=0
      END IF
      END IF
!------------------------------------------------------------ Pass 4
      if(1500<time(2))then
      tt=op*(i-1500)*pc
      deo=0.1143
      v=0.0015
      pe=deo*3.14
      po=pe/v
      pc=360/po
      Q=1180
      op=3.14/180
      yp=(coords(2)*cos(tt)+coords(3)*sin(tt))-deo/2
      zp=coords(2)*sin(tt)-coords(3)*cos(tt)
      if(jltyp.eq.1)then
      if(zp<0)then
      WA=sqrt(3.0)
      WB=(3.14)**(3/2)
      wr=6*WA*FF*Q/(A*B*CF*WB)
      wt=EXP(-3*(x**2/(A**2)))
      wy=EXP(-3*(yp**2/(B**2)))
      WU=EXP(-3*(zp**2/(CF**2)))
      flux(1)=WR*WT*WY*WU
      end if
      if(zp>0)then
      WA=3**(1/2)
      WB=(3.14)**(3/2)
      wr=6*WA*Fr*Q/(A*B*Cr*WB)
      wt=EXP(-3*(x**2/(A**2)))
      wy=EXP(-3*(yp**2/(B**2)))
      WU=EXP(-3*(zp**2/(Cr**2)))
      flux(1)=WR*WT*WY*WU
      END IF
      END IF
      END IF
!------------------------------------------------------------ cooling 4
      end do
      RETURN
      END
```

```
      SUBROUTINE FILM(H,SINK,TEMP,KSTEP,KINC,TIME,NOEL,NPT,
     1 COORDS,JLTYP,FIELD,NFIELD,SNAME,NODE,AREA)
C
      INCLUDE 'ABA_PARAM.INC'
C
      DIMENSION H(2),TIME(2),COORDS(3),FIELD(NFIELD)
      CHARACTER*80 SNAME
      do i=1,time(2)
      do j=50,temp
      if(temp<500)then
      sink=25
      h(1)=0.068*temp
      else
      h(1)=0.231*temp-81.5
      end if
      end do
      end do
      RETURN
      END
```

APPANDIX A.4:

Subroutine codes for modeling heat input and heat loss in PIPE 4.

```
      SUBROUTINE DFLUX(FLUX,SOL,KSTEP,KINC,TIME,NOEL,NPT,COORDS,
     1 JLTYP,TEMP,PRESS,SNAME)
C
      INCLUDE 'ABA_PARAM.INC'
C
      DIMENSION FLUX(2),TIME(2),COORDS(3)
      CHARACTER*80 SNAME
      A=0.006
      B=0.005
      CR=0.015
      CF=0.005
      FR=1.15
      FF=0.85
      EF=0.73
      do i=1,time(2)
!------------------- ----------------------------- --------   Pass 1
      if(time(2)<529.25)then
      tt=op*i*pc
      deo=0.09164
      v=0.000545
      pe=deo*3.14
      po=pe/v
      pc=360/po
      Q=991
      op=3.14/180
      yp=(coords(2)*cos(tt)+coords(3)*sin(tt))-deo/2
      zp=coords(2)*sin(tt)-coords(3)*cos(tt)
      if(jltyp.eq.1)then
      if(zp<0)then
      WA=sqrt(3.0)
      WB=(3.14)**(3/2)
      wr=6*WA*FF*Q/(A*B*CF*WB)
      wt=EXP(-3*(x**2/(A**2)))
      wy=EXP(-3*(yp**2/(B**2)))
      WU=EXP(-3*(zp**2/(CF**2)))
      flux(1)=WR*WT*WY*WU
      end if
      if(zp>0)then
      WA=3**(1/2)
      WB=(3.14)**(3/2)
      wr=6*WA*Fr*Q/(A*B*Cr*WB)
      wt=EXP(-3*(x**2/(A**2)))
      wy=EXP(-3*(yp**2/(B**2)))
      WU=EXP(-3*(zp**2/(Cr**2)))
      flux(1)=WR*WT*WY*WU
      END IF
      END IF
      END IF
!------------------------------------------------------------ cooling 1
      if(529.25<time(2) .AND. 700>time(2))then
      pe=deo*3.14
      v=0.001
      po=pe/v
      pc=360/po
      Q=0
      if(zp<0)then
      flux(1)=0
      end if
      if(zp>0)then
      flux(1)=0
      END IF
```

```
      END IF

! ------------------------------------------------------------ pass 2
      if(700<time(2) .AND. 953.53>time(2))then
      tt=op*(i-700)*pc
      deo=0.09684
      v=0.0012
      pe=deo*3.14
      po=pe/v
      pc=360/po
      Q=1092
      op=3.14/180
      yp=(coords(2)*cos(tt)+coords(3)*sin(tt))-deo/2
      zp=coords(2)*sin(tt)-coords(3)*cos(tt)
      if(jltyp.eq.1)then
      if(zp<0)then
      WA=sqrt(3.0)
      WB=(3.14)**(3/2)
      wr=6*WA*FF*Q/(A*B*CF*WB)
      wt=EXP(-3*(x**2/(A**2)))
      wy=EXP(-3*(yp**2/(B**2)))
      WU=EXP(-3*(zp**2/(CF**2)))
      flux(1)=WR*WT*WY*WU
      end if
      if(zp>0)then
      WA=3**(1/2)
      WB=(3.14)**(3/2)
      wr=6*WA*Fr*Q/(A*B*Cr*WB)
      wt=EXP(-3*(x**2/(A**2)))
      wy=EXP(-3*(yp**2/(B**2)))
      WU=EXP(-3*(zp**2/(Cr**2)))
      flux(1)=WR*WT*WY*WU
      END IF
      END IF
      END IF
!------------------------------------------------------------ cooling 2
      if(953.53<time(2) .AND. 1100>time(2))then
      pe=deo*3.14
      v=0.0015
      po=pe/v
      pc=360/po
      Q=0
      if(zp<0)then
      flux(1)=0
      end if
      if(zp>0)then
      flux(1)=0
      END IF
      END IF
! ------------------------------------------------------------ pass 3
      if(1100<time(2) .AND. 1313.7>time(2))then
      tt=op*(i-1100)*pc
      deo=0.10202
      v=0.0015
      pe=deo*3.14
      po=pe/v
      pc=360/po
      Q=1180
      op=3.14/180
      yp=(coords(2)*cos(tt)+coords(3)*sin(tt))-deo/2
      zp=coords(2)*sin(tt)-coords(3)*cos(tt)
      if(jltyp.eq.1)then
      if(zp<0)then
      WA=sqrt(3.0)
      WB=(3.14)**(3/2)
      wr=6*WA*FF*Q/(A*B*CF*WB)
      wt=EXP(-3*(x**2/(A**2)))
```

```
      wy=EXP(-3*(yp**2/(B**2)))
      WU=EXP(-3*(zp**2/(CF**2)))
      flux(1)=WR*WT*WY*WU
      end if
      if(zp>0)then
      WA=3**(1/2)
      WB=(3.14)**(3/2)
      wr=6*WA*Fr*Q/(A*B*Cr*WB)
      wt=EXP(-3*(x**2/(A**2)))
      wy=EXP(-3*(yp**2/(B**2)))
      WU=EXP(-3*(zp**2/(Cr**2)))
      flux(1)=WR*WT*WY*WU
      END IF
      END IF
      END IF
!------------------------------------------------------------ COOLING 3
      if(1313.7<time(2) .AND. 1500>time(2))then
      pe=deo*3.14
      v=0.0015
      po=pe/v
      pc=360/po
      Q=0
      if(zp<0)then
      flux(1)=0
      end if
      if(zp>0)then
      flux(1)=0
      END IF
      END IF
! ------------------------------------------------------------ PASS5
      if(1500<time(2) .AND. 1668.4>time(2))then
      tt=op*(i-1500)*pc
      deo=0.1072
      v=0.002
      pe=deo*3.14
      po=pe/v
      pc=360/po
      Q=1180
      op=3.14/180
      yp=(coords(2)*cos(tt)+coords(3)*sin(tt))-deo/2
      zp=coords(2)*sin(tt)-coords(3)*cos(tt)
      if(jltyp.eq.1)then
      if(zp<0)then
      WA=sqrt(3.0)
      WB=(3.14)**(3/2)
      wr=6*WA*FF*Q/(A*B*CF*WB)
      wt=EXP(-3*(x**2/(A**2)))
      wy=EXP(-3*(yp**2/(B**2)))
      WU=EXP(-3*(zp**2/(CF**2)))
      flux(1)=WR*WT*WY*WU
      end if
      if(zp>0)then
      WA=3**(1/2)
      WB=(3.14)**(3/2)
      wr=6*WA*Fr*Q/(A*B*Cr*WB)
      wt=EXP(-3*(x**2/(A**2)))
      wy=EXP(-3*(yp**2/(B**2)))
      WU=EXP(-3*(zp**2/(Cr**2)))
      flux(1)=WR*WT*WY*WU
      END IF
      END IF
      END IF
!------------------------------------------------- cooling 5
      if(1668.4<time(2) .AND. 1800>time(2))then
      pe=deo*3.14
      v=0.002
      po=pe/v
```

```
      pc=360/po
      Q=0
      if(zp<0)then
      flux(1)=0
      end if
      if(zp>0)then
      flux(1)=0
      END IF
      END IF
! ------------------------------------------------------------ pass 5
      if(1800<time(2) .AND. 2009.5>time(2))then
      tt=op*(i-1800)*pc
      deo=0.1143
      v=0.001713
      pe=deo*3.14
      po=pe/v
      pc=360/po
      Q=1180
      op=3.14/180
      yp=(coords(2)*cos(tt)+coords(3)*sin(tt))-deo/2
      zp=coords(2)*sin(tt)-coords(3)*cos(tt)
      if(jltyp.eq.1)then
      if(zp<0)then
      WA=sqrt(3.0)
      WB=(3.14)**(3/2)
      wr=6*WA*FF*Q/(A*B*CF*WB)
      wt=EXP(-3*((x+0.005)**2/(A**2)))
      wy=EXP(-3*(yp**2/(B**2)))
      WU=EXP(-3*(zp**2/(CF**2)))
      flux(1)=WR*WT*WY*WU
      end if
      if(zp>0)then
      WA=3**(1/2)
      WB=(3.14)**(3/2)
      wr=6*WA*Fr*Q/(A*B*Cr*WB)
      wt=EXP(-3*(x**2/(A**2)))
      wy=EXP(-3*(yp**2/(B**2)))
      WU=EXP(-3*(zp**2/(Cr**2)))
      flux(1)=WR*WT*WY*WU
      END IF
      END IF
      END IF
!------------------------------------------------------------ cooling 5
      if(2009.5<time(2) .AND. 2100>time(2))then
      pe=deo*3.14
      v=0.001713
      po=pe/v
      pc=360/po
      Q=0
      if(zp<0)then
      flux(1)=0
      end if
      if(zp>0)then
      flux(1)=0
      END IF
      END IF
!------------------------------------------------------------------ Pass 6
      if(2100<time(2))then
      tt=op*(i-2100)*pc
      deo=0.1143
      v=0.001713
      pe=deo*3.14
      po=pe/v
      pc=360/po
      Q=1180
      op=3.14/180
      yp=(coords(2)*cos(tt)+coords(3)*sin(tt))-deo/2
```

```
      zp=coords(2)*sin(tt)-coords(3)*cos(tt)
      if(jltyp.eq.1)then
      if(zp<0)then
      WA=sqrt(3.0)
      WB=(3.14)**(3/2)
      wr=6*WA*FF*Q/(A*B*CF*WB)
      wt=EXP(-3*(x**2/(A**2)))
      wy=EXP(-3*(yp**2/(B**2)))
      WU=EXP(-3*(zp**2/(CF**2)))
      flux(1)=WR*WT*WY*WU
      end if
      if(zp>0)then
      WA=3**(1/2)
      WB=(3.14)**(3/2)
      wr=6*WA*Fr*Q/(A*B*Cr*WB)
      wt=EXP(-3*(x**2/(A**2)))
      wy=EXP(-3*(yp**2/(B**2)))
      WU=EXP(-3*(zp**2/(Cr**2)))
      flux(1)=WR*WT*WY*WU
      END IF
      END IF
      END IF
!------------------------------------------------------- cooling final
      end do
      RETURN
      END

       SUBROUTINE FILM(H,SINK,TEMP,KSTEP,KINC,TIME,NOEL,NPT,
     1 COORDS,JLTYP,FIELD,NFIELD,SNAME,NODE,AREA)
C
      INCLUDE 'ABA_PARAM.INC'
C
      DIMENSION H(2),TIME(2),COORDS(3),FIELD(NFIELD)
      CHARACTER*80 SNAME
      do i=1,time(2)
      do j=50,temp
      if(temp<500)then
      sink=25
      h(1)=0.068*temp
      else
      h(1)=0.231*temp-81.5
      end if
      end do
      end do
      RETURN
      END
```

APPANDIX A.5:

Hardness measurments in all pipes after welding.

PIPE 1: 2”-sch number 40					PIPE 2: 2”-Sch Number 80				
Regions	Point 1	Point 2	Point 3	MEAN	Regions	Point 1	Point 2	Point 3	MEAN
Unaffceted zone	131	135	130	132	Unaffceted zone	118	129	118	122
HAZ 1	166	149	153	156	HAZ 1	131	134	128	131
FZ 1	129	129	126	128	FZ 1	117	136	131	128
HAZ 2	160	146	156	154	HAZ 2	150	136	138	142
HAZ over-lapping zone	160	159	167	165	HAZ over-lapping zone	149	149	152	150
HAZ 3	135	134	147	139	HAZ 3	139	142	139	140
FZ 2	126	122	123	124	FZ 2	137	140	137	138
HAZ 4	130	130	138	133	HAZ 4	145	148	151	148
PIPE 3: 4”-Sch number 80					PIPE 4: 4”-Sch number 120				
Regions	Point 1	Point 2	Point 3	MEAN	Regions	Point 1	Point 2	Point 3	MEAN
Unaffceted zone	122	125	129	125	Unaffceted zone	131	135	130	132
HAZ 1	130	125	143	132	HAZ 1	166	149	153	156
FZ 1	128	138	130	132	FZ 1	129	129	126	128
HAZ 2	147	148	138	144	HAZ 2	160	146	156	154
HAZ over-lapping zone	142	140	138	140	HAZ over-lapping zone	160	159	167	165
HAZ 3	132	138	138	136	HAZ 3	135	134	147	140
FZ 2	131	131	139	133	FZ 2	126	122	123	124
HAZ 4	131	132	135	133	HAZ 4	130	140	136	135

CURRICULUM VITAE

Name Surname : **Arash ARMANFAR**

Place and Date of Birth : **Tabriz Iran, 1990**

E-Mail : **Armanfar.arash@gmail.com**

EDUCATION

- **B.Sc.** : **Sahand Technical University, indsutial metallurgy**
- **M.Sc.** : **Istanbul Technical University, Mechanical Design**